

# Perspectives on advances in high-capacity, free-space communications using multiplexing of orbital-angular-momentum beams

Cite as: APL Photonics 6, 030901 (2021); <https://doi.org/10.1063/5.0031230>

Submitted: 06 October 2020 • Accepted: 31 January 2021 • Published Online: 17 March 2021

 Alan E. Willner, Zhe Zhao, Cong Liu, et al.

## COLLECTIONS

 This paper was selected as an Editor's Pick



View Online



Export Citation



CrossMark

## ARTICLES YOU MAY BE INTERESTED IN

[Orbital angular momentum of light for communications](#)

Applied Physics Reviews 8, 041312 (2021); <https://doi.org/10.1063/5.0054885>

[Orbital angular momentum communications based on standard multi-mode fiber \(invited paper\)](#)

APL Photonics 6, 060804 (2021); <https://doi.org/10.1063/5.0049022>

[Enhancing the modal purity of orbital angular momentum photons](#)

APL Photonics 5, 070802 (2020); <https://doi.org/10.1063/5.0005597>

**APL Photonics**

Applications now open for the  
**Early Career Editorial Advisory Board**

[Learn more and submit](#)

# Perspectives on advances in high-capacity, free-space communications using multiplexing of orbital-angular-momentum beams

Cite as: APL Photon. 6, 030901 (2021); doi: [10.1063/5.0031230](https://doi.org/10.1063/5.0031230)

Submitted: 6 October 2020 • Accepted: 31 January 2021 •

Published Online: 17 March 2021



Alan E. Willner,<sup>1,a)</sup>  Zhe Zhao,<sup>1</sup> Cong Liu,<sup>1</sup> Runzhou Zhang,<sup>1</sup> Haoqian Song,<sup>1</sup> Kai Pang,<sup>1</sup> Karapet Manukyan,<sup>1</sup>  Hao Song,<sup>1</sup> Xinzhou Su,<sup>1</sup> Guodong Xie,<sup>1</sup> Yongxiong Ren,<sup>1</sup> Yan Yan,<sup>1</sup> Moshe Tur,<sup>2</sup> Andreas F. Molisch,<sup>1</sup> Robert W. Boyd,<sup>3,4</sup>  Huibin Zhou,<sup>1</sup> Nanzhe Hu,<sup>1</sup> Amir Minoofar,<sup>1</sup> and Hao Huang<sup>1</sup>

## AFFILIATIONS

<sup>1</sup>Department of Electrical Engineering, University of Southern California, Los Angeles, California 90089, USA

<sup>2</sup>School of Electrical Engineering, Tel Aviv University, Ramat Aviv 69978, Israel

<sup>3</sup>Department of Physics, University of Ottawa, Ottawa, Ontario K1N 6N5, Canada

<sup>4</sup>The Institute of Optics, University of Rochester, Rochester, New York 14627, USA

<sup>a)</sup> Author to whom correspondence should be addressed: [willner@usc.edu](mailto:willner@usc.edu)

## ABSTRACT

Beams carrying orbital-angular-momentum (OAM) have gained much interest due to their unique amplitude and phase structures. In terms of communication systems, each of the multiple independent data-carrying beams can have a different OAM value and be orthogonal to all other beams. This paper will describe the use of multiplexing and the simultaneous transmission of multiple OAM beams for enhancing the capacity of communication systems. We will highlight the key advances and technical challenges in the areas of (a) free-space and fiber communication links, (b) mitigation of modal coupling and channel crosstalk effects, (c) classical and quantum systems, and (d) optical and radio frequency beam multiplexing.

© 2021 Author(s). All article content, except where otherwise noted, is licensed under a Creative Commons Attribution (CC BY) license (<http://creativecommons.org/licenses/by/4.0/>). <https://doi.org/10.1063/5.0031230>

## I. INTRODUCTION AND OVERVIEW

In 1992, Allen *et al.*<sup>1</sup> reported that orbital angular momentum (OAM) can be carried by an optical vortex beam. This beam has a unique spatial structure such that its amplitude has a ring-like doughnut profile and the phase front “twists” in a helical fashion as it propagates. The number of  $2\pi$  phase changes in the azimuthal direction represents the OAM mode order, and beams with different OAM values can be orthogonal to each other (Fig. 1). Such structured beams are a subset of the Laguerre–Gaussian ( $LG_{lp}$ ) modal basis set in free space, which has two modal indices: (1)  $l$  represents the number of  $2\pi$  phase shifts in the azimuthal direction and the size of the ring grows with  $l$  and (2)  $p + 1$  represents the number of concentric amplitude rings.<sup>2,3</sup> This orthogonality enables multiple independent optical beams to be multiplexed, spatially co-propagate, and be demultiplexed—all with minimal inherent crosstalk.<sup>1,3,4</sup>

This orthogonality is crucially beneficial for a communications system. It implies that multiple independent data-carrying optical beams can be multiplexed and simultaneously transmitted in either free-space or fiber, thereby multiplying the system’s data capacity by the total number of beams (Fig. 2). Moreover, since all the beams are in the same frequency band, the system’s spectral efficiency (i.e., bits/s/Hz) is also increased. These multiplexed orthogonal OAM beams are a form of mode-division multiplexing (MDM), which itself is a subset of space-division multiplexing (SDM).<sup>5–7</sup>

MDM shares similarities with wavelength-division multiplexing (WDM) in which multiple independent data-carrying optical beams of different wavelengths can be multiplexed and simultaneously transmitted. WDM revolutionized optical communication systems and is ubiquitously deployed worldwide. Importantly, MDM is generally compatible with and can

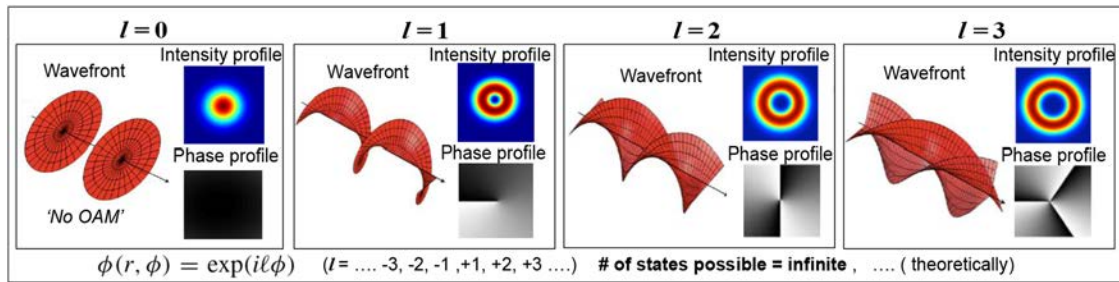


**FIG. 1.** The wavefronts, intensity profiles, and phase profiles of OAM modes  $l = 0, 1, 2$ , and  $3$ . The OAM mode with a nonzero order has a donut-shaped intensity profile and helical phase front. The size of the ring in the intensity profile grows with  $l$ . We note that  $p + 1$  represents the number of concentric amplitude rings and  $p = 0$  is shown in the figure. Reproduced with permission from Yao and Padgett, *Adv. Opt. Photon.* **3**, 161 (2011). Copyright 2011 Optical Society of America.

complement WDM such that each of the many wavelengths can contain many orthogonal structured beams and thus dramatically increase data capacity.<sup>7,9,10</sup>

The field of OAM-based optical communications (i) is considered young and rich with scientific and technical challenges, (ii) is promising for technological advances and applications, and (iii) has produced much research worldwide such that the number of publications per year has grown significantly.<sup>11</sup> Capacities, distances, and numbers of data channels have all increased, and approaches for mitigating degrading effects have produced encouraging results.<sup>4,11,12</sup>

In this paper, we discuss the evolution of several sub-fields in OAM-based optical communications. We describe advances and perspectives on different aspects of this field, including (a) free-space optical (FSO) communication links; (b) modal coupling effects and channel crosstalk mitigation techniques; (c) airborne and underwater systems; (d) quantum communications; (e) radio-frequency, millimeter-wave (mm-wave), and THz links; and (f) fiber-based systems. We note that this article will generally assume OAM multiplexed “free-space classical” optical communications as the basic default system, and separate subsections will be dedicated to the topics that deviate from this system (e.g., quantum, radio frequencies, or fiber). The intent of this article is to give a flavor of the advances as well as the growing interest in this field. To explore more about this, see the references at the end.

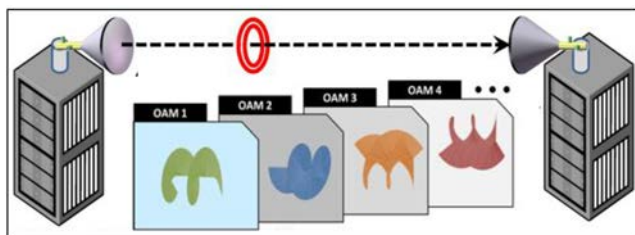


**FIG. 2.** Concept of OAM multiplexed FSO links. Multiple OAM beams are co-axially transmitted through free space, each carrying an independent data stream.<sup>8</sup> Reproduced with permission from Yan *et al.*, *Nat. Commun.* **5**, 4876 (2014). Copyright 2014 Macmillan Publishers.

## II. OAM-BASED FREE-SPACE MDM SYSTEMS

### A. High-capacity OAM-multiplexed communication links

OAM multiplexing has the potential to increase the total transmission rates in optical communication systems due to its ability to multiplex and simultaneously transmit multiple data-carrying channels on different OAM beams. As each OAM beam carrying an independent data stream co-propagates with other OAM beams, the spectral efficiency of the system (i.e., bits/s/Hz) scales with the number of OAM beams utilized for multiplexing. As such, OAM beams can be carried on both orthogonal polarizations, and polarization-division multiplexing (PDM) can also be applied to further double the spectral efficiency of the system. The first use of OAM multiplexing for MDM communication links resulted in an FSO link that multiplexed four different OAM modes on two polarizations, with an aggregated data rate of 1.37 Tbit/s.<sup>7</sup> As shown in Fig. 3, on one polarization, four Gaussian beams carrying independent data channels (Data1, Data3, Data5, and Data7) were transformed into four OAM modes (OAM1, OAM2, OAM3, and OAM4) by adding different phase patterns. Conjugated phase patterns were used at the receiver to convert the OAM-carrying beams back into Gaussian beams. By utilizing PDM, four additional data channels (Data2, Data4, Data6, and Data8) were multiplexed and carried by the same OAM modes (OAM1, OAM2, OAM3, and OAM4) on the other polarization, resulting in eight independent data channels on the same wavelength. This increased the spectral efficiency of the system eightfold.

Moreover, WDM can be utilized to further increase the capacity of OAM multiplexed FSO links. The concept of combining OAM-multiplexing, PDM, and WDM for capacity enhancement is presented in Fig. 4. OAM-multiplexing and PDM are combined and carried on the same frequency [Figs. 4(a) and 4(b)], and other independent data channels can be transmitted/received utilizing the other frequencies on the same OAM modes and both polarizations [Fig. 4(c)]. As the OAM multiplexing and PDM are compatible with WDM, utilizing  $M$  different carrier frequencies allows us to further increase the aggregated link capacity by  $M$  times. Thus, the combination of  $N$ -OAM based MDM, PDM, and  $M$ -frequency based WDM can increase the aggregated data rate of an FSO communication link by  $2 \times N \times M$  times as compared to using a single Gaussian beam

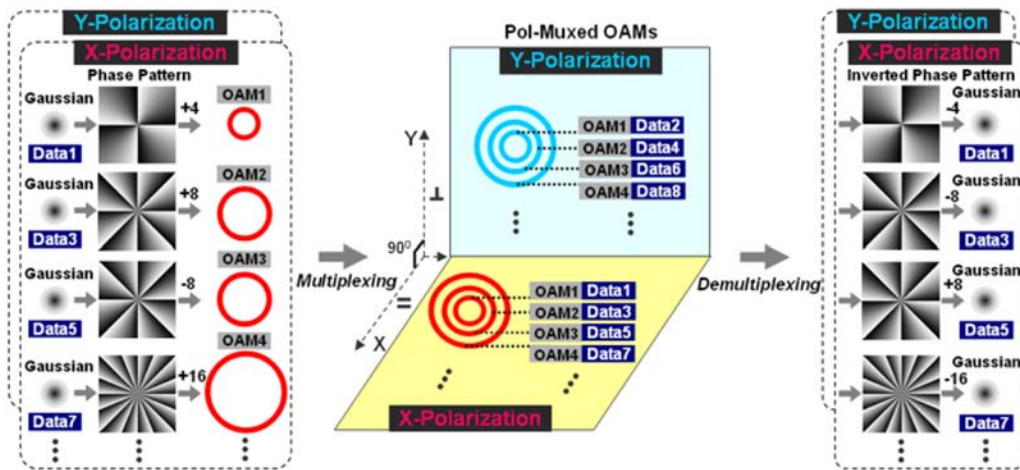


**FIG. 3.** The concept of multiplexing/demultiplexing four information-carrying OAM beams (left panel) combined with PDM (middle panel) to achieve a 1.37 Tbit/s aggregated rate. For demultiplexing, an OAM beam is converted back into a Gaussian beam that has high intensity at the center (right panel, second column), which can be separated from other “doughnut shaped” OAM beams by a spatial filter. Pol-Muxed: polarization-multiplexed. Reproduced with permission from Wang *et al.*, Nat. Photonics **6**, 488 (2012). Copyright 2012 Nature Research.

on a single frequency and polarization.<sup>9,10</sup> One demonstration of such a system combined 12 OAM modes, two polarizations, and 42 wavelengths, resulting in a total of 1008 data channels each carrying 100-Gbit/s data, to achieve an aggregated rate of 100.8 Tbit/s in the laboratory.<sup>9</sup> Figure 4(d) shows the observed optical spectrum of a single OAM beam ( $l = +10$ ) that carries the WDM signals.<sup>9</sup> Another work reported a demonstration of 26-OAM mode-multiplexing over 368 WDM and polarization-multiplexed with an aggregate data rate of 1.036 Pbit/s.<sup>10</sup>

The experimental demonstrations of OAM-multiplexed communication links in the laboratory were generally conducted over short distances of  $\sim 1$  m. In recent years, there have been several experiments that investigated the potential of using OAM beams to achieve long-distance FSO links in the field environment:<sup>13–15</sup>

- (i) A 120-m FSO communication link with a 400-Gbit/s data rate based on four-OAM multiplexing; each OAM beam carries 100-Gbit/s quadrature phase-shift keying (QPSK) modulated data channels.<sup>13</sup>
- (ii) A 260-m FSO data transmission link between two buildings using OAM multiplexing and 16-quadrature-amplitude-modulation (16-QAM) signals with an 80-Gbit/s aggregated bit rate.<sup>14</sup>

The expansion of an OAM-based link over much longer distances might give rise to several challenges, including the divergence of the OAM beams, system pointing and misalignment, and atmospheric turbulence effects. Significant efforts have been made to achieve such links over longer distances. An FSO link based on the OAM encoding scheme was demonstrated over a distance of  $\sim 143$  km between two islands.<sup>15</sup> An OAM-based encoding scheme can be achieved by sequentially transmitting different OAM beams, each representing a data symbol, within each time slot. Compared to a binary signal, which has two possible data bit values of “0” and “1,” an  $M$ -ary OAM encoding signal may have many values

ranging from “0” to “ $M - 1$ .” The number of data bits per unit time can reach  $\log_2 M$ , and thus, the data capacity in each channel can be increased.

Figure 5(a) shows the link layout for sending and receiving the OAM modes in the above-mentioned 143-km link.<sup>15</sup> The observed patterns of four different OAM mode superpositions are shown in Figs. 5(b)–5(e). Under the relatively weak turbulence, the lobed modal structure was visible for mode superpositions with  $l = \{-1, +1\}$ ,  $\{-2, +2\}$ , or  $\{-3, +3\}$ . In order to recover the encoded data, an artificial neural network-based pattern recognition algorithm was used to distinguish images of different OAM mode superpositions. The received mode superpositions could be identified with an accuracy of  $>80\%$  up to OAM mode order  $l = 3$ , and the decoded message had an error rate of 8.33%. The results indicate that the free-space transmission of OAM modes over a 100-km-scale distance is feasible.

## B. Two-dimensional modal basis sets

Although there has been significant interest in OAM as a modal basis set for MDM communications, what is the rationale for choosing OAM over other types of modes? On a fundamental level, MDM requires that you can efficiently combine and separate different modes, so almost any complete orthogonal basis set could work. Indeed, many different types of modes were demonstrated in free-space and fiber, including Hermite–Gaussian (HG), LG, and linearly polarized (LP) modes.<sup>5,7,16–20</sup> In discussions with Boyd and Padgett,<sup>21</sup> two practical issues seemed to emerge as reasons that one “might” prefer OAM modes (as a subset of LG modes) to other modal basis sets:

- (i) OAM modes are round, and free-space optical components are readily available in round form.
- (ii) It is important to maintain interchannel orthogonality and minimize crosstalk. This can be accomplished by fully



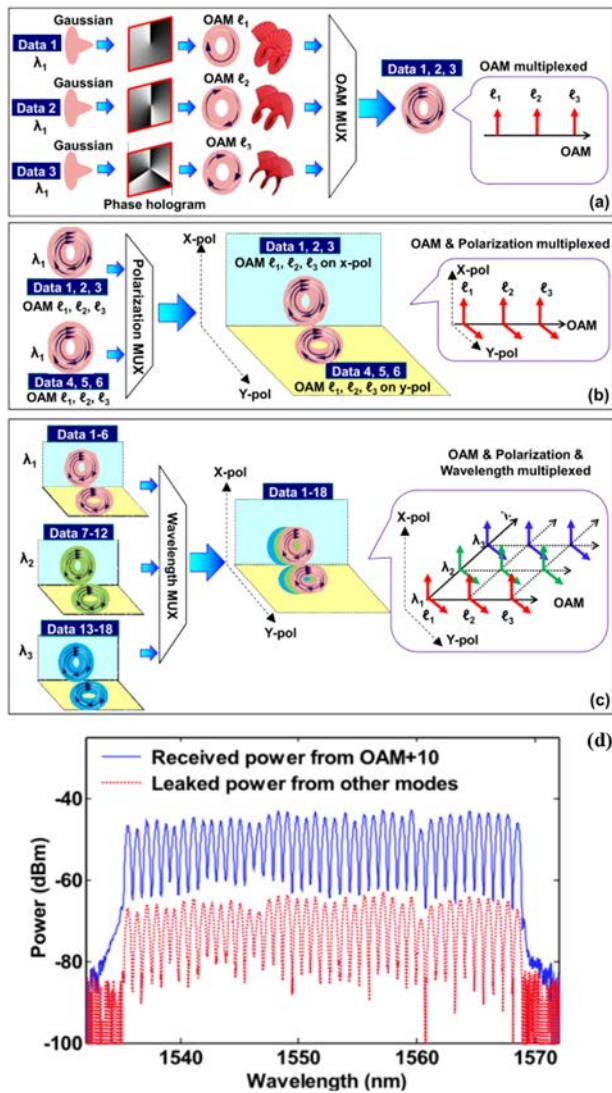


**FIG. 4.** (a)–(c) The concept of combining OAM multiplexing with PDM and WDM to increase the link capacity. (a) Multiplexing multiple data channels on OAM-carrying beams. (b) Combining OAM multiplexing with PDM. (c) Combining OAM multiplexing and PDM with WDM, 12 OAM modes, 2 polarizations, and 42 wavelengths were multiplexed in total to achieve a 100.8 Tbit/s aggregated data rate. (d) Measured optical spectrum of the WDM signal carried on the OAM beam with  $l = +10$ . Reproduced with permission from Huang *et al.*, Opt. Lett. **39**, 197 (2014). Copyright 2014 Optical Society of America.

capturing the specific parameter that defines the modal orthogonality. For a case in which different channels can be defined by different OAM  $l$  values, the channel and mode can be fully determined by azimuthally capturing a full  $360^\circ$  circle no matter the size of the round aperture.<sup>22,23</sup>

Structured beams from a modal basis set can generally be described by two modal indices such that the beam can be fully described by these coordinates. For example, LG modes have  $l$

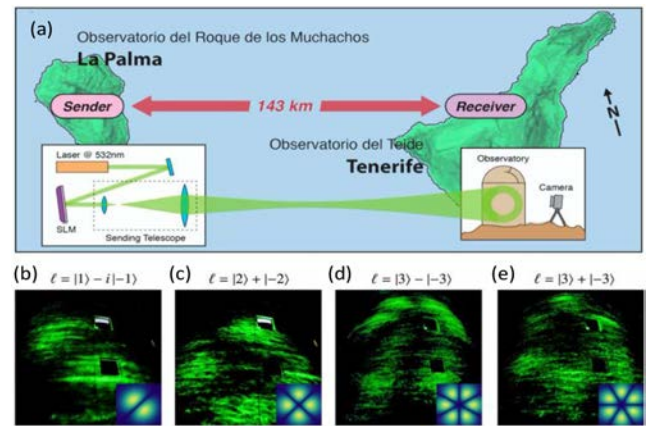


**FIG. 5.** (a) The layout sketch of an OAM-encoded link over a distance of  $\sim 143$  km. At the transmitter, OAM beams were generated by shining Gaussian beams on to a spatial light modulator (SLM). A telescope was used to collimate OAM beams for decreasing the divergence effects. [(b)–(e)] Examples of superposed OAM (vortex) modes observed at the receiver. The intensity profiles were distorted mainly due to the atmospheric turbulence effects. Reproduced with permission from Krenn *et al.*, Proc. Natl. Acad. Sci. U.S.A. **113**, 13648 (2016). Copyright 2016 United States National Academy of Sciences.

(azimuthal) and  $p$  (radial) components, whereas HG beams have  $n$  (horizontal) and  $m$  (vertical) components. OAM modes are a subset of a full LG modal basis set, which can be characterized by two indices: the radial index  $p$  and the azimuthal index  $l$ , as shown in Fig. 6. The electrical field of an LG beam can be represented by<sup>2,18</sup>

$$LG_{\ell,p}(r, \phi, l, p, \omega_0) = \frac{\sqrt{2}r^{|l|}}{\omega_0^{|l|+1}} \exp\left(-\frac{r^2}{\omega_0^2} + il\phi\right) LP_p^{|l|}\left(\frac{2r^2}{\omega_0^2}\right), \quad (1)$$

where  $\omega_0$  is the beam waist,  $LP_p^{|l|}$  is the generated Laguerre polynomials, and  $(r, \phi)$  is the cylindrical coordinate. However, the vast majority of publications on MDM-based FSO communications

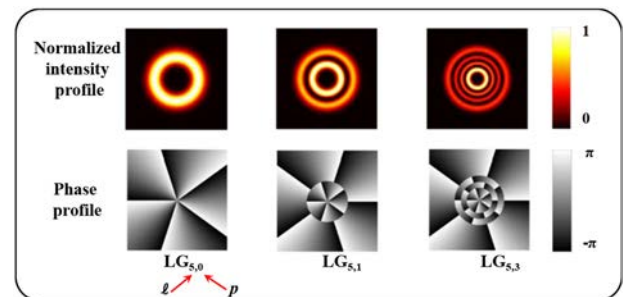


**FIG. 6.** Intensity and phase profiles of LG beams with non-zero radial index  $p$  and azimuthal index  $l$ . The values of  $p + 1$  and  $l$  represent the number of rings in the intensity profile for the non-zero  $l$  value and the number of  $2\pi$  phase changes along the azimuthal direction in the phase profile. LG beams with different pairs of indices  $(l, p)$  are orthogonal to each other.<sup>24</sup> Reproduced with permission from Li *et al.*, Proc. J. Opt. Soc. Am. B **34**, 1 (2017). Copyright 2017 Optical Society of America.

utilized only a change in a single modal index. Specifically, each beam commonly had a different  $l$  value but the same  $p = 0$  value.<sup>7,8,10,13,15,23</sup> LG beams with different  $p$  values can also be utilized in MDM FSO links. For example, there has been an experimental demonstration of a 200-Gbit/s MDM link based on the multiplexing of LG modes with the same  $l$  value but different  $p$  values.<sup>18</sup> It should be noted that these works utilized one-dimensional modal basis sets, which means that they only varied one of the two modal indices ( $l, p$ ). While this one-dimensional system can accommodate many orthogonal beams, a system designer could also use the other beam modal index in order to possibly achieve a larger two-dimensional set of data channels. This two-dimensional approach was shown experimentally for LG and HG beams.<sup>17,18</sup> It is important to note that a significant challenge is the sufficient capture of the beam at the receiver aperture to ensure accurate phase recovery and orthogonality along both indices.<sup>18</sup>

Theoretically, LG beams with different pairs of indices ( $l, p$ ) are orthogonal to each other. Therefore, extending the one-dimensional modal basis sets (e.g., LG beams with only  $l$  or  $p$  index changing) to two-dimensional ones (e.g., LG beams with both  $l$  and  $p$  indices changing) could provide a larger two-dimensional modal space for orthogonal data-carrying channels and increase the transmission capacity of a communication link. A fourfold multiplexing of LG modes was experimentally demonstrated to achieve a 400-Gbit/s communication link.<sup>17</sup> In this experiment, a two-dimensional LG modal set was used and both modal indices ( $l, p$ ) were varied. In addition, four HG modes were utilized to achieve such a four-channel MDM link [Fig. 7(a)], and the effects of aperture size as well as lateral and rotational misalignments on the crosstalk performance were also investigated.<sup>17</sup> Due to different symmetric properties of LG modes and HG modes, they might present different crosstalk performances under different misalignments in the MDM link. It was found that (1) a limited-size aperture at the receiver causes power loss for both LG and HG beams, (2) a lateral misalignment between the transmitter and receiver causes crosstalk for LG beams, while HG beams with a zero  $m$  or  $n$  index are more tolerant to lateral misalignment due to the axial symmetry, and (3) a rotational misalignment causes crosstalk for HG beams but does not tend to influence LG modes due to their circular symmetry, as shown in Fig. 7(b).

### III. BASIC CHALLENGES AND EFFECTS FOR OAM-BASED MDM COMMUNICATION SYSTEM

A key issue in almost any MDM communication system is dealing with intermodal power coupling and deleterious inter-data-channel crosstalk. There are many causes of modal coupling and crosstalk, including the following for OAM-multiplexed FSO communication links, as shown in Fig. 8:

- Turbulence:** atmospheric turbulence can cause a phase distortion at different cross-sectional locations of a propagating beam. Given this phase change distribution in a changing environment, power can couple from the intended mode into others dynamically (e.g., perhaps changes of the order of milliseconds).<sup>26–29</sup>
- Misalignment:** misalignment between the transmitter and receiver means that the receiver aperture is not coaxial with the incoming OAM beams. In order to operate an OAM-multiplexed link, one needs to know which modes are being transmitted. A receiver aperture that captures power around the center of the beam will recover the full azimuthal phase change and know which  $l$  mode was transmitted. However, a limited-size receiver aperture that is off-axis will not recover the full phase change and inadvertently “thinks” that some power resides in other  $l$  and/or  $p$  modes.<sup>30</sup>
- Divergence:** FSO beams of higher OAM orders diverge faster than lower-order OAM beams, thus making it difficult to fully capture the higher-order OAM beams with a limited-sized receiver aperture. Power loss occurs if the beam power is not fully captured, but even modal coupling can occur due to the truncation of the beam’s radial profile. This truncation can result in power being coupled to some other LG beams with different  $p$  values ( $p$  modes).<sup>30–32</sup>
- Mode multiplexing/demultiplexing:** mode multiplexing and demultiplexing is another challenge in OAM-multiplexing based systems, which requires a scalable unitary transformation. Various studies have addressed this challenge, including (a) multi-plane light conversion (MPLC) achieved by shaping the wavefront of the light at multiple propagating distances to accomplish mode conversion between Gaussian beams at different locations and different HG/LG beams,<sup>33,34</sup> (b)

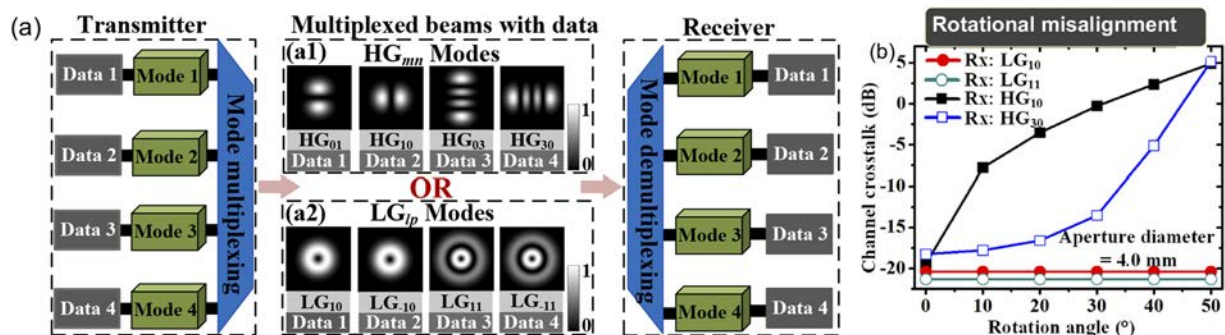


**FIG. 7.** (a) Concept of an MDM link using four LG modes or four HG modes, each carrying 100 Gbit/s signal (i.e., 400 Gbit/s in total). (b) Measured crosstalk for each mode when all four HG or LG modes are transmitted with various receiver rotation angles. Reproduced with permission from Pang *et al.*, Opt. Lett. **43**, 3889 (2018). Copyright 2018 Optical Society of America.

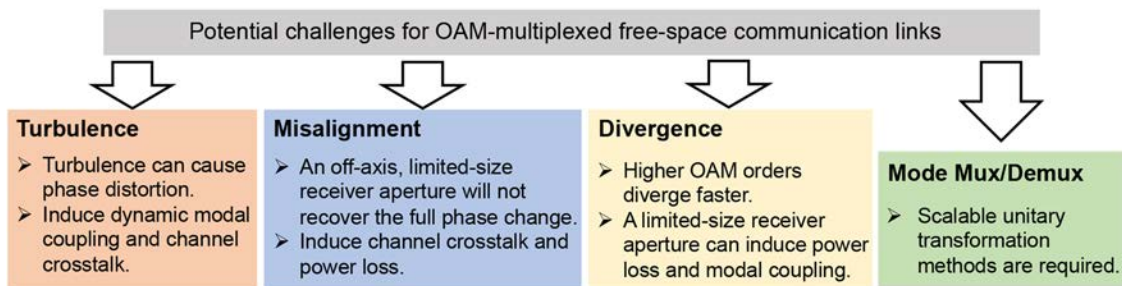


**FIG. 8.** Potential challenges for an OAM-multiplexed FSO communication link. Turbulence effects distort the beam phase front, thus inducing dynamic modal coupling and channel crosstalk. A misaligned, off-axis, limited-size receiver aperture would not recover the full phase change and will induce channel crosstalk and power loss. Beam divergence effects could be important for a long-distance transmission: higher-order OAM-carrying beams diverge faster, which could lead to power loss and modal coupling due to the limited receiver size. The mode multiplexing and demultiplexing requires methods to achieve scalable unitary transformation. Mux: multiplexing. Demux: demultiplexing.

log-polar-based mode sorter that geometrically transforms the spiral spatial phase of OAM beams into a tilted spatial phase,<sup>35,36</sup> and (c) designing refractive index distribution of the fiber designed to achieve in-fiber mode conversion from the fundamental mode to the vector mode.<sup>37</sup>

It should also be mentioned that (i) modal coupling “tends” to be higher to the adjacent modes and (ii) separating data channels with a larger modal differential can help in alleviating the problem.<sup>28,38,39</sup> Of course, larger modal separation leads to larger beam divergence, so a trade-off analysis is usually recommended.

### A. Atmospheric turbulence

Atmospheric turbulence is one important challenge that needs to be considered for an OAM-multiplexed FSO communication system. Inhomogeneities in the temperature and pressure of the atmosphere can lead to variations in the refractive index along the transmission path.<sup>27,40</sup> As in an OAM-multiplexed link, the orthogonality among multiple co-propagating OAM beams depends on their helical phase front, turbulence-induced refractive index

inhomogeneities can cause intermodal crosstalk between different data channels with different OAM orders, as they can easily distort the phase front of OAM beams [Fig. 9(a)].<sup>28,41,42</sup>

The effects of atmospheric turbulence on the performance of OAM-multiplexed systems have been experimentally evaluated in the laboratory in several ways.<sup>27–29</sup> One example of the emulation of atmospheric effects in the laboratory is shown in Fig. 9(a), which presents the concept of using a rotating phase plate to emulate the turbulence effects. The phase screen plate is mounted on a rotating stage and placed in the optical path of the beams. On the rotating plate, the pseudorandom phase distribution obeys Kolmogorov spectrum statistics.<sup>28</sup> The strength of the emulated turbulence effect generally depends on the Fried parameter  $r_0$  and the beam size that is incident on the plate. In order to evaluate the turbulence effects, the modal crosstalk is characterized by measuring the power of the distorted beam in each OAM mode. Figure 9(b) presents the normalized power distribution among the neighboring OAM modes under weak and strong turbulences for an OAM +3 transmitted beam. It is shown that under the weak turbulence, the majority of the power is still in the transmitted OAM mode (i.e., OAM +3), and only a small part of the power is coupled to other neighboring OAM modes.

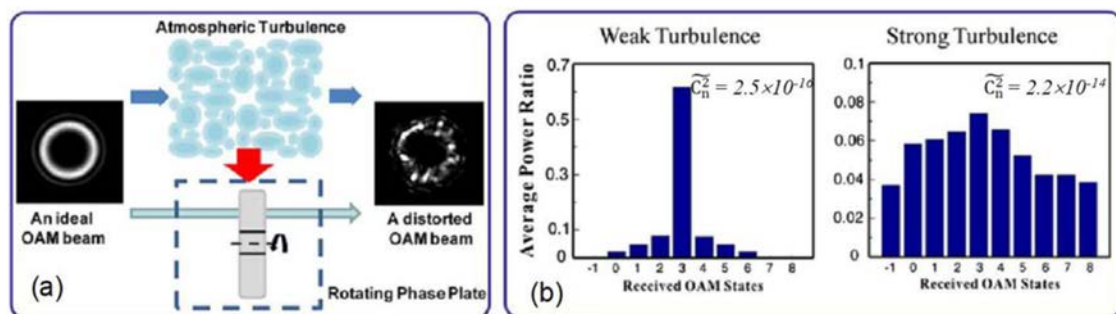


**FIG. 9.** (a) A rotating phase plate is used as an atmospheric turbulence emulator. The OAM beam intensity profile is distorted after passing through the phase plate. (b) Measured power distribution of an OAM beam after passing through the turbulence emulator with weak and strong atmospheric turbulence, respectively.  $\tilde{C}_n^2$ : the effective atmospheric structure constant—larger  $\tilde{C}_n^2$  indicates stronger turbulence effects. Reproduced with permission from Ren *et al.*, Opt. Lett. 38, 4062 (2013). Copyright 2013 Optical Society of America.



However, as the turbulence strength increases, the power coupling into other OAM modes becomes higher, which could induce severe signal fading and crosstalk.

## B. Misalignment

The efficient multiplexing and de-multiplexing of OAM beams requires coaxial propagation and reception of the transmitted modes. Unlike the case of using Gaussian beams, any misalignment between the transmitter and receiver apertures or only partial collection of the OAM beams at the receiver would result not only in power loss but also, more severely, in interchannel crosstalk (i.e., power coupled to other modes). In an ideal OAM multiplexed communication link, the transmitter and receiver would be perfectly aligned [i.e., the center of the receiver would overlap the center of the transmitted beam, and the receiver plane would be perpendicular to the line connecting their centers, as shown in Fig. 10(a)]. However, due to jitter and vibration of the transmitter/receiver platform, the transmitter and receiver may have relative lateral shift (i.e., lateral displacement) or angular shift (i.e., receiver angular error), as depicted in Figs. 10(b) and 10(c), respectively. Both types of misalignment may lead to the degradation of system performance.

Figures 10(d) and 10(e) illustrate the effect of the lateral displacement and receiver angular error when only OAM +3 is transmitted with a beam diameter of 3 cm.<sup>30</sup> Given a fixed link distance of 100 m, the power coupling into other modes increases with an increase in the lateral displacement or receiver angular error, whereas the power on OAM +3 (i.e., the transmitted mode) decreases. This is because a larger lateral/angular displacement causes a larger mismatch between the received OAM beams and the receiver. The power coupled to OAM +2 and OAM +4 is greater than that of OAM +1 and OAM +5 due to their smaller mode

spacing from OAM +3. This indicates that a system with larger mode spacing is more tolerant to the lateral displacement.

## C. Beam divergence

For a communication link, it is preferable to collect as much signal power as possible at the receiver to ensure a sufficient signal-to-noise ratio (SNR). Based on diffraction theory, a light beam diverges while propagating in free space. Since optical elements usually have limited-size apertures, the diverged beam might be too large to be fully collected, resulting in signal power loss. For an OAM-multiplexed link, the transmitted beams with higher OAM orders diverge faster than lower-order OAM beams. This makes it difficult to fully capture them with a limited-size receiver aperture, which leads to signal power loss. Moreover, a limited-size receiver aperture can also degrade the orthogonality between  $p$  modes,<sup>30–32,43</sup> as shown in Fig. 11. Truncation might occur in the beam's radial profile, and this could potentially induce a modal coupling from the desired mode to some other LG beams with different  $p$  values ( $p$  modes).<sup>31,43</sup> For an MDM link using LG modes with different  $p$  values, this modal coupling might cause channel crosstalk. The divergence effect of an LG beam mainly depends on the frequency, transmission distance, beam waist at the transmitter, and mode indices. Therefore, in order to reduce the signal power loss and channel crosstalk, the key parameters related to the beam divergence need to be carefully considered when designing an OAM-based link.

## IV. ADVANCES IN CROSSTALK MITIGATION FOR OAM-MULTIPLEXED COMMUNICATION LINKS

Crosstalk mitigation is one of the key challenges for OAM multiplexed communications. Various optical and digital techniques

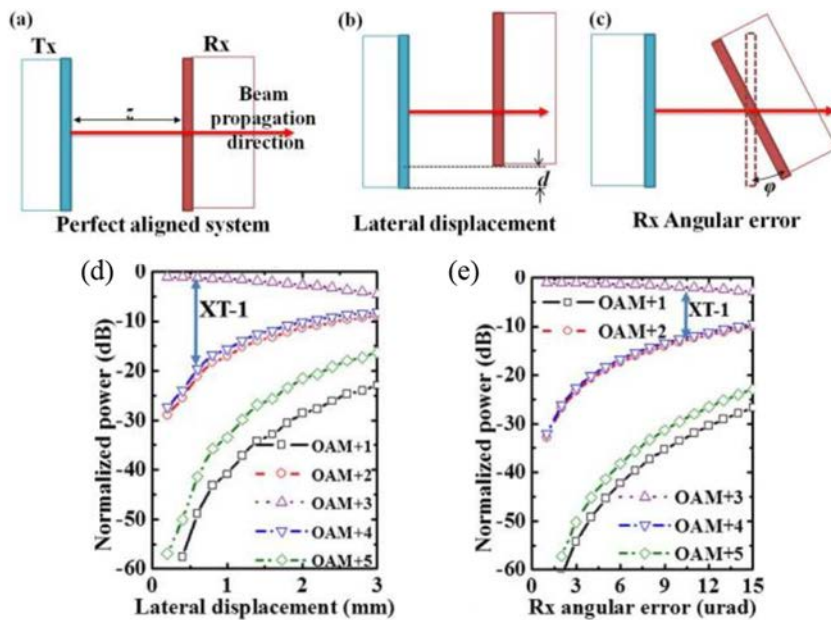


**FIG. 10.** (a)–(c) Three different cases of alignment between the transmitter and receiver: (a) a perfectly aligned system, (b) a system with lateral displacement, and (c) a system with receiver angular error. [(d) and (e)] Simulated power distribution among different OAM modes as a function of (c) lateral displacement and (d) receiver angular error over a 100-m link for which only OAM 3 is transmitted. The transmitted beam size is 3 cm and the receiver aperture size is 4.5 cm. Tx—transmitter, Rx—receiver,  $z$ —transmission distance,  $d$ —displacement, and  $\phi$ —angular error. XT-1—crosstalk between neighboring OAM modes. Reproduced with permission from Xie *et al.*, *Optica* 2, 357 (2015). Copyright 2015 Optical Society of America.



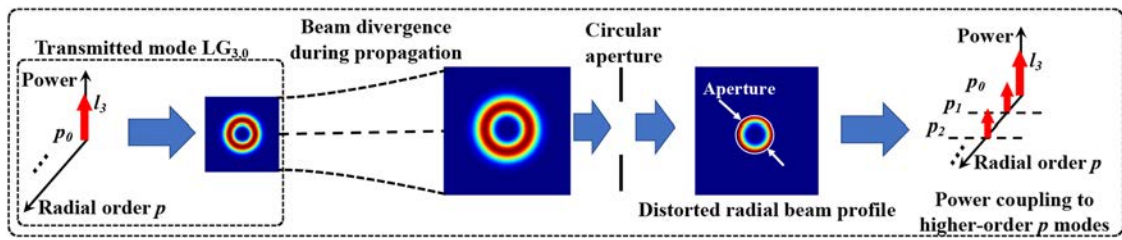


**FIG. 11.** The concept of circular aperture truncation effects to OAM-carrying beams due to OAM beam divergence and limited-size receiver aperture. OAM  $l = 3$  mode (i.e., LG  $l = 3, p = 0$  mode) is shown as an example: the beam diverges during propagation, and the radial beam profile is distorted at the receiver side due to the circular truncation, which induces a modal coupling from the transmitted mode to some other LG modes with different higher order  $p$  values.

have been proposed for crosstalk mitigation in OAM-multiplexed links, as shown in Fig. 12. Conventional approaches for crosstalk mitigation include the following:

- (i) **Adaptive optics (AO):** AO, such as by using digital micromirrors, spatial light modulators (SLMs), or multi-plane-light converters (MPLCs), can mitigate modal crosstalk.<sup>34,44–46</sup> For example, if atmospheric turbulence causes a certain phase distortion on an optical beam, an SLM at the receiver can induce an inverse phase function to partially undo the effects of turbulence.<sup>45</sup> Typically, there could be a feedback loop such that a data or probe beam is being monitored for dynamic changes and the new phase function is fed to an SLM, as shown in Fig. 13(a1). With the usage of the AO system, the distorted OAM beams can be efficiently compensated, as shown in Figs. 13(a2) and 13(a3).
- (ii) **Electrical digital signal processing (DSP):** crosstalk due to modal coupling has many similarities to crosstalk that occurs in multiple-transmitter-multiple-receiver (i.e., multiple-input multiple-output, MIMO) radio systems,<sup>47,48</sup> as shown in Fig. 13(b1). Multiple optical modes are similar to parallel radio frequency (RF) beams that experience crosstalk. Similar to electronic DSP that can undo much of the crosstalk in MIMO RF systems, these DSP approaches could also be used for mitigating OAM modal crosstalk.<sup>49</sup> With MIMO equalization, the error vector magnitude (EVM) of

the four channels can be improved, as shown in Figs. 13(b2) and 13(b3). The EVM is a parameter that could quantify the performance of a communication system, and a lower EVM value indicates a better signal quality.

In the conventional receiving system for an OAM multiplexed link, mitigating OAM crosstalk and channel demultiplexing are typically achieved separately.<sup>33,45</sup> As mentioned above, AO and DSP can be applied to mitigate crosstalk. Additionally, MPLC has been demonstrated as a scalable and reconfigurable mode demultiplexer.<sup>33,34</sup> It might be desirable to mitigate crosstalk and demultiplex channels simultaneously. Recently, it was shown that the wavefront-shaping-and-diffusing method could simultaneously mitigate turbulence and demultiplex channels, but this approach involves some power loss.<sup>50–52</sup> Another approach is to use an MPLC to mitigate crosstalk and demultiplex channels, and this method theoretically has no inherent power loss.<sup>53,54</sup> Such an approach was demonstrated experimentally using a single MPLC to simultaneously mitigate the turbulence-induced crosstalk and demultiplex two channels carried by OAM modes.<sup>54</sup> As shown in Fig. 14(a), input coaxial OAM beams having different mode orders are converted to Gaussian beams at different output positions using the cascaded phase patterns calculated by the wavefront-matching method.<sup>33,34</sup> To mitigate turbulence-induced crosstalk, the patterns are updated by combining the genetic algorithm with the wavefront matching method. Figure 14(b) shows the measured crosstalk matrix without

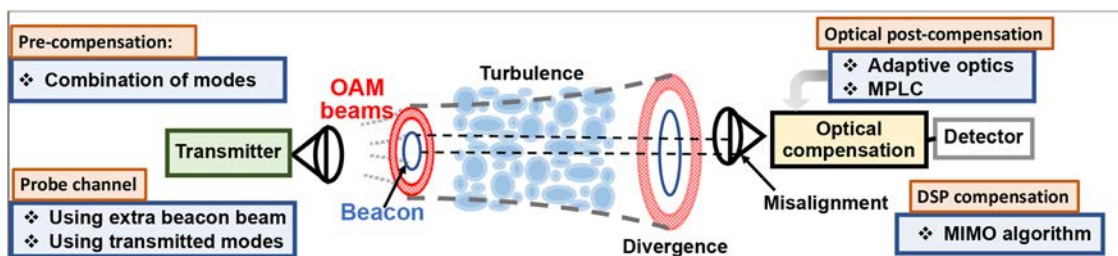


**FIG. 12.** Different crosstalk mitigation approaches for an OAM-multiplexed FSO link. An extra beacon beam or the transmitted data-carrying modes can be used as a probing channel to characterize the distortion from the turbulent media. Reports have shown various approaches for crosstalk mitigation: Optical approaches (e.g., AO, combinations of modes, and MPLC-based method) have been utilized to mitigate crosstalk at the transmitter and/or receiver, while MIMO method has been utilized to mitigate crosstalk at the receiver in the electrical domain.

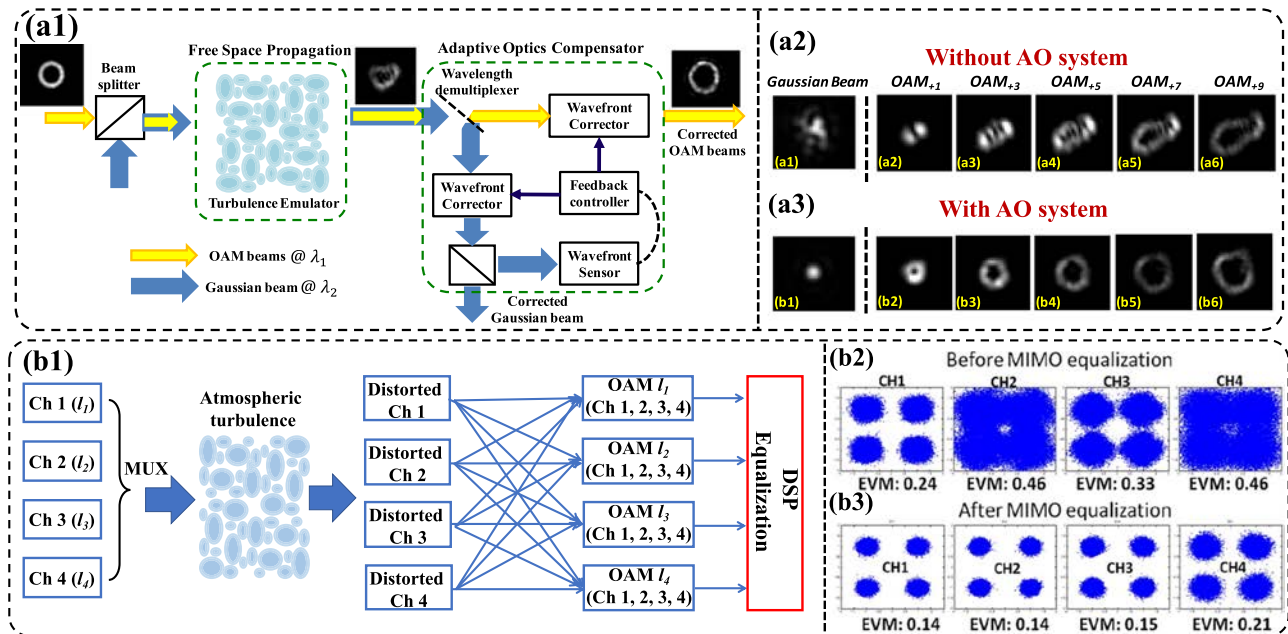


**FIG. 13.** (a) Concept of using AO for crosstalk mitigation. The wavefront sensor measures the phase front distortion of the beam and the corresponding correction pattern is loaded on the wavefront corrector to undo the distortion. [(a2) and (a3)] The measured OAM beam profiles after being transmitted through the turbulent medium without and with the AO compensation. With the AO system, the distorted OAM beams can be efficiently compensated. (b1) Concept of using MIMO DSP to mitigate the modal crosstalk in the electrical domain. [(b2) and (b3)] Measured EVMs of the OAM-multiplexed channels. With MIMO equalization, the EVMs of the four channels can be improved. Reproduced with permission from Ren *et al.*, *Optica* 1, 376 (2014) and Huang *et al.*, *Opt. Lett.* 39, 4360 (2014). Copyright 2014 Optical Society of America.

turbulence and without and with crosstalk mitigation under the turbulence for various OAM multiplexing cases of  $\ell = \{-1, +1\}$  and  $\ell = \{-1, +2\}$ . Without crosstalk mitigation, the crosstalk performance for  $\ell = \{-1, +1\}$  and  $\ell = \{-1, +2\}$  is increased by >13.1 dB and >9.2 dB, respectively, compared with the cases without turbulence, respectively. Applying crosstalk mitigation results in mitigation of >11.4 dB and >7.2 dB for  $\ell = \{-1, +1\}$  and  $\ell = \{-1, +2\}$ , respectively. These results show that a single MPLC could be

reconfigured to achieve simultaneous crosstalk mitigation and channel demultiplexing for different OAM multiplexing cases.

Besides an increasing array of potential methods for crosstalk mitigation in OAM-based links, advanced technologies including the artificial neural network-based pattern recognition algorithm<sup>15</sup> are also considered. As with most issues, cost and complexity will play a key role in determining which, if any, mitigating approach should be used. In this section, we will discuss the recent advances

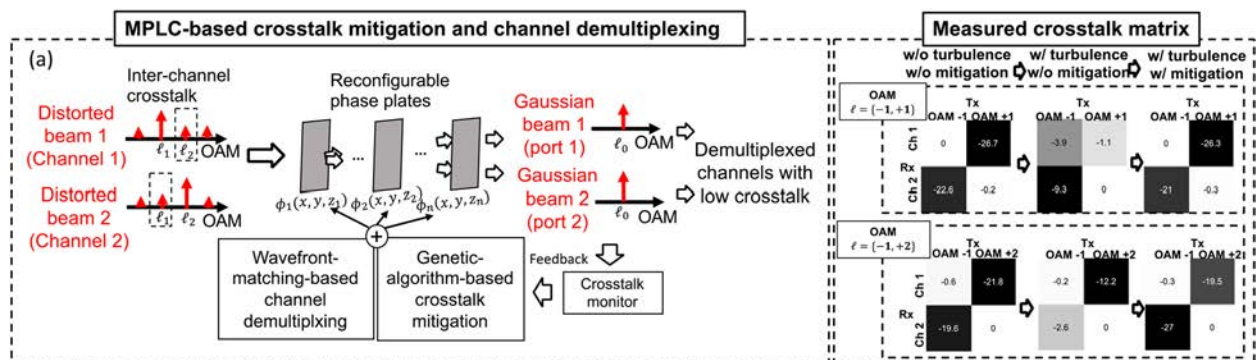


**FIG. 14.** (a) The concept of the MPLC-based crosstalk mitigation and channel demultiplexing. (b) Measured crosstalk matrix for channel demultiplexing without turbulence, without and with MPLC-based crosstalk mitigation under the turbulence. Reproduced with permission from Song *et al.*, *2020 Optical Fiber Communications Conference (OFC) (OSA, 2020)*, p. W1G.3. Copyright 2020 Optical Society of America.

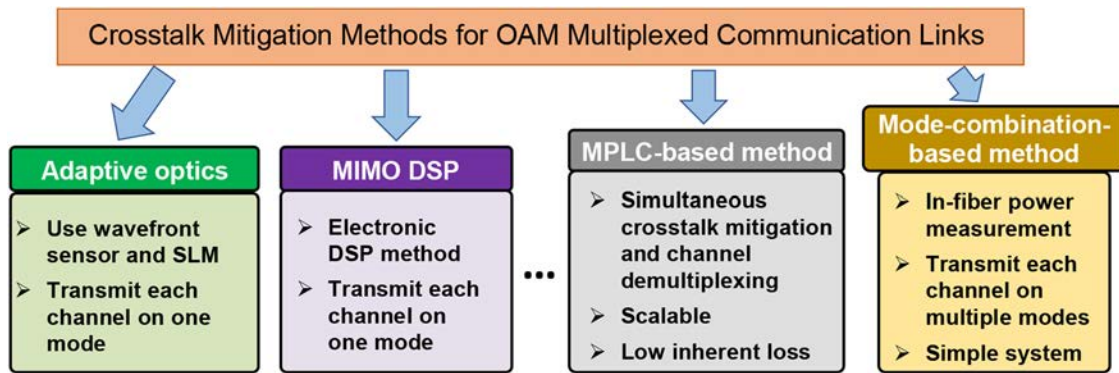


FIG. 15. Crosstalk mitigation methods for OAM-multiplexed communication links.

in crosstalk mitigation approaches for OAM-multiplexed FSO communications, as shown in Fig. 15. Specifically, we will mainly discuss approaches based on transmitting the coherent combination of multiple OAM modes at the transmitter for turbulence mitigation.

### A. Mode-combination-based mitigation

Aside from the conventional crosstalk mitigation approaches, it would be beneficial to develop an alternative approach that (a) only needs in-fiber power measurement instead of using wavefront sensors to measure the spatial amplitude and phase profile of the optical beams and (b) can mitigate the crosstalk from other data channels without recovering all the data channels at the receiver. Recently, multiple optical approaches have been developed to address these issues.<sup>43,55–58</sup> These approaches are based on the transmission or detection of a combination of multiple spatial modes. The steps to achieve this include (i) measuring the complex transmission matrix of the imperfect MDM links using the modal power distribution, (ii) calculating the phase patterns to generate/detect different combinations of multiple modes based on the measured transmission matrix, and (iii) applying the phase patterns to mitigate the crosstalk.<sup>43,55</sup> This method is feasible because a structured beam can be decomposed into a set of LG modes that carry OAM, as shown in Fig. 16. The coefficient of each LG mode in the decomposition can be complex, containing both amplitude and phase information. Therefore, one can control the amplitude and phase shift for each LG mode and coherently combine all modes to generate a structured beam that performs the desired function.

An optical turbulence mitigation approach based on mode combination has been recently demonstrated.<sup>55</sup> The experimental results for 200-Gbit/s two-OAM-multiplexed links showed that the inter-channel crosstalk could be reduced by >10 dB. The concept of turbulence compensation using mode combination is illustrated in Fig. 17(a). At the transmitter side, the inverse transmission matrix is applied using a compensation phase pattern at the transmitter for each channel, which results in the signal from each transmitted channel being carried by the combination of multiple

(e.g., 2) OAM modes with designed complex weights. The weights are calculated based on the inverse of the complex transmission matrix under the corresponding turbulence realization, and such combinations of OAM modes could perform the inverse function of turbulence-induced crosstalk. When the beams from the two channels are transmitted through the turbulence, the signals on the two transmitted modes will couple to their neighboring modes and experience coherent interference on those modes. Therefore, the channels could have little power on the designated modes due to their destructive interference and relatively high power on the others. By receiving the mode on which the undesired channel has little power, the desired channel can be recovered with little inter-channel crosstalk. The same concept can be applied to recover the second channel when receiving another mode. As an example, the compensation phase patterns used for beam generation in channel A and the intensity profiles of the generated beams are shown in Fig. 17(b).

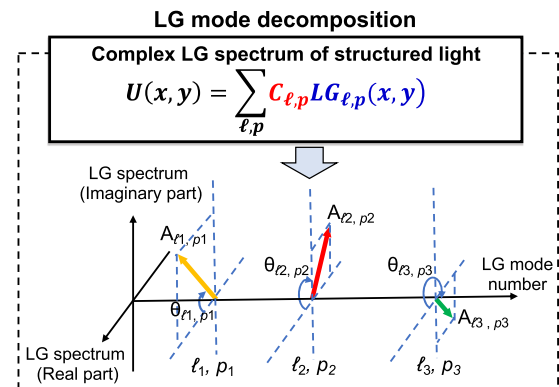
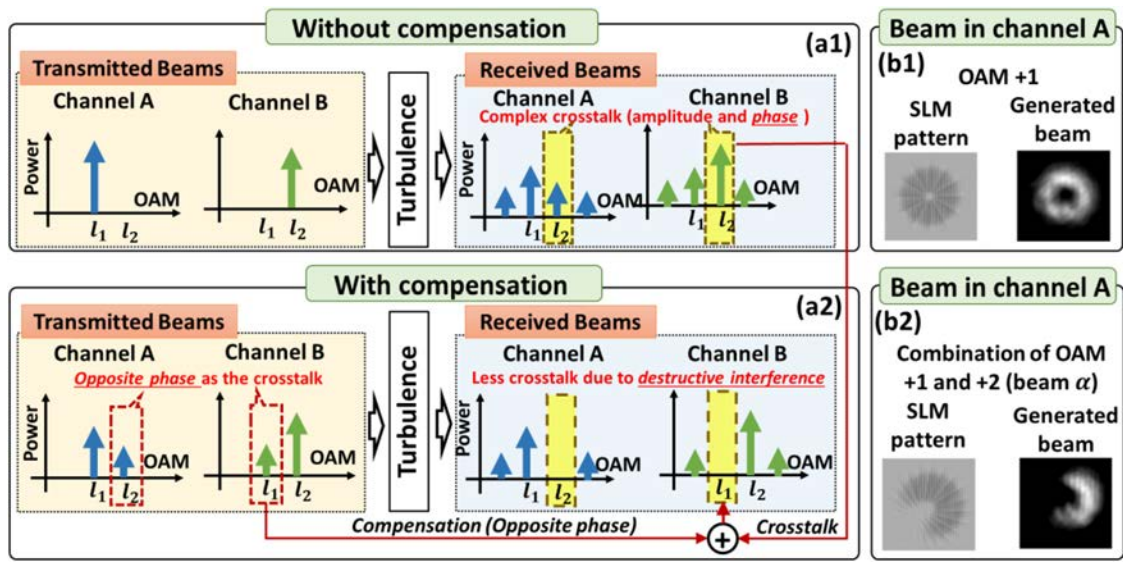


FIG. 16. The concept of the LG mode decomposition and the complex LG spectrum. A structured beam can be decomposed into a set of LG modes that carry OAM. The complex coefficient, i.e., each element of the complex LG spectrum, can be calculated using the overlapped integral between the electric fields of the structured beam and each LG mode. We can control the amplitude ( $A$ ) and phase shift ( $\theta$ ) for each LG mode and coherently combine all modes to generate a structured beam.





**FIG. 17.** (a) The concept of the turbulence compensation utilizing the inverse transmission matrix method: (a1) transmitting pure OAM modes without applying the compensation approach and (a2) transmitting the combination of OAM modes while compensating for the turbulence effects. (b) An example of the SLM patterns and the generated beams intensity profiles in the cases of transmission (b1) without compensation and (b2) with compensation. Reproduced with permission from Song *et al.*, J. Light. Technol. **38**, 82 (2020). Copyright 2020 Optical Society of America.

This approach was demonstrated for two-OAM ( $l = +1$  and  $l = +2$ ) multiplexed channels each carrying a 100-Gbit/s QPSK signal.<sup>55</sup> When the compensation approach was applied, the transmitted channels A and B carried beams  $\alpha$  and  $\beta$ , respectively, which were combinations of OAM  $l = +1$  and  $l = +2$ . The receivers for channels A and B recovered the signals on OAM modes  $l = +1$  and  $l = +2$ , respectively. The results of this demonstration are shown in Fig. 18. The back-to-back case is illustrated in Fig. 18(a1). As shown in Fig. 18(a2), with the turbulence effect, the inter-channel crosstalk increases to  $-8.7$  dB and  $-5.5$  dB for channels A and B, respectively, in the absence of the compensation, and this crosstalk decreases to  $-22.1$  dB and  $-17.8$  dB for the two channels with the

compensation. The bit error rate (BER) performance for the channels is shown in Fig. 18(b). By applying pre-compensation phase patterns in the link, the BER performance can be improved. These results indicate that transmitting a combination of multiple OAM modes with designed mode weights instead of a single OAM mode could improve the performance of an OAM-multiplexed link by reducing the crosstalk.

In addition, the mode-combination-based approach was also utilized to mitigate the effect of the limited-size aperture or a misalignment in an MDM link.<sup>43</sup> This can be achieved by transmitting each data channel on a combination of multiple LG modes, as shown in Fig. 19(a). The complex transmission matrix  $\mathbf{H}$  of the link can

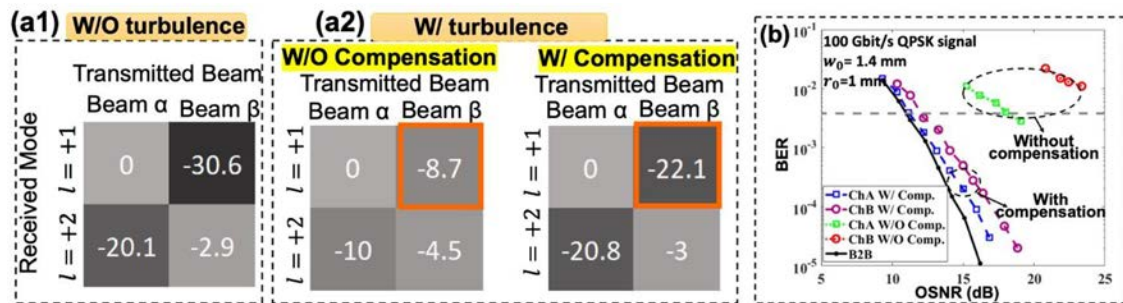


**FIG. 18.** (a1) and (a2) The measured normalized transmission intensity matrices and (b) BER measurements for the channels without and with compensation. In the demonstration, channel A receives OAM  $l = +1$ , while channel B receives OAM  $l = +2$ . In the link without compensation, channels A and B transmit OAM  $l = +1$  and  $l = +2$ , respectively. Beams  $\alpha$  and  $\beta$  are the combinations of OAM  $+1$  and  $+2$  transmitted by channels A and B, respectively, when the compensation is applied. Reproduced with permission from Song *et al.*, J. Light. Technol. **38**, 82 (2020). Copyright 2020 Optical Society of America.

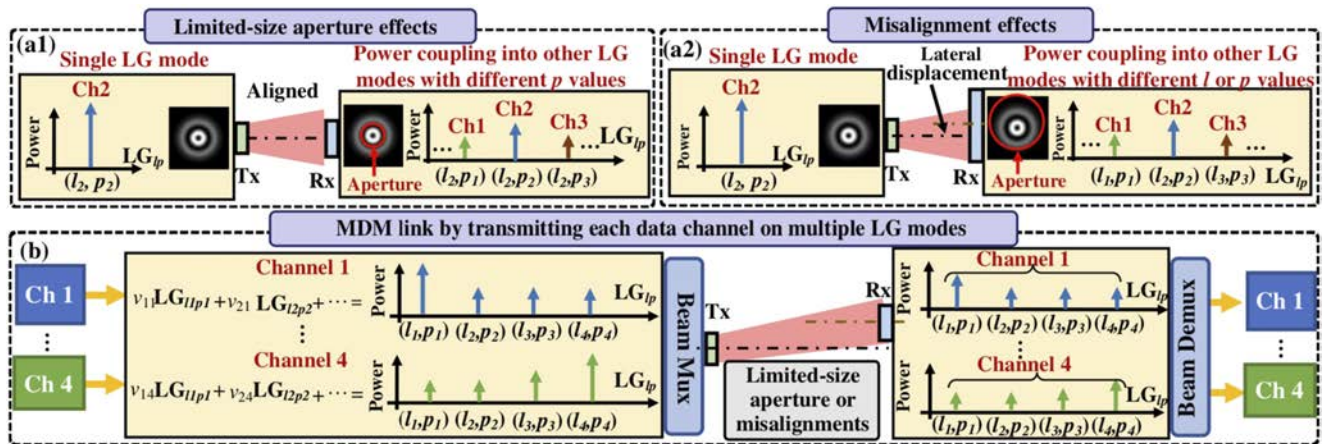


**FIG. 19.** (a) Concept of (a1) limited-size aperture and (a2) misalignment effects on an FSO link using LG modes. (b) Concept diagram of transmitting each data channel on a designed beam that is a combination of multiple LG modes to mitigate the effects of the limited-size aperture or misalignments in an MDM link. Ch—channel, Tx—transmitter, and Rx—receiver. Reproduced with permission from Pang et al., 2020 Optical Fiber Communications Conference and Exhibition (OFC) (OSA, 2020), pp. 1–3. Copyright 2020 Optical Society of America.

be factorized by singular value decomposition (SVD) and written as  $\mathbf{H} = \mathbf{U} \cdot \Sigma \cdot \mathbf{V}^*$ . At the transmitter side, the orthogonal beams are generated by using complex combinations of multiple LG modes, of which the complex weights (amplitude and phase) are given by the orthogonal column vectors of  $\mathbf{V}$ . After passing through a given link ( $\mathbf{H}$ ) with a limited-size aperture or misalignments, the resulting beams on different channels would still be mutually orthogonal. Such beams are composed of multiple LG modes, the complex weights of which are the orthogonal row vectors multiplied by singular values in the matrix  $\Sigma$ . These resulting beams are still orthogonal to each other and thus can be demultiplexed with little crosstalk based on the orthogonal row vectors of the inversed  $\mathbf{U}$  matrix [Fig. 19(b)]. Besides the orthogonalization, intensity profiles of the transmitted beams would also be spatially shaped, which might simultaneously reduce the power loss caused by the limited-size aperture or the misalignment.

The above approach was experimentally demonstrated in a four-channel multiplexed link with each channel carrying a 100-Gbit/s QPSK signal.<sup>43</sup> The results for crosstalk mitigation under horizontal displacements are shown in Fig. 20 as examples. Figure 20(a) presents that when transmitting data channels on pure LG modes with different  $p$  values ( $LG_{10}$ ,  $LG_{11}$ ), the crosstalk becomes larger with an increase in the horizontal displacement. However, when using the orthogonal beams (beams 1 and 2) that are generated by using designed complex combinations of  $LG_{10}$  and  $LG_{11}$  modes, the crosstalk for both channels could be  $< -27$  dB with the displacement. Figure 20(b) shows the case of LG modes with different  $l$  values ( $LG_{10}$ ,  $LG_{-10}$ ) under various displacements. The crosstalk of ( $LG_{10}$ , or  $LG_{-10}$ ) increases with the displacement, but for the designed orthogonal beams (composed of  $LG_{10}$  and  $LG_{-10}$ ), it could stay at a relatively low level ( $< -17$  dB) in association with the displacement for both channels. These results indicate that by simultaneously

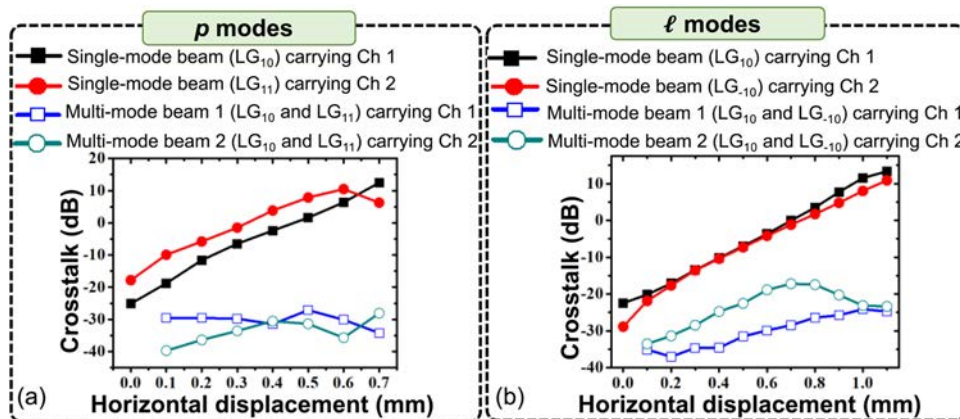


**FIG. 20.** Experimental results of the simultaneous orthogonalization and shaping of the multiple LG beams method for crosstalk mitigation: displacement-induced channel crosstalk under various horizontal displacements when transmitting data channels on (a) pure LG modes with different  $p$  values ( $LG_{10}$ ,  $LG_{11}$ ) or designed orthogonal beams and (b) pure LG modes with different  $l$  values ( $LG_{10}$ ,  $LG_{-10}$ ) or designed orthogonal beams. Reproduced with permission from Pang et al., 2020 Optical Fiber Communications Conference and Exhibition (OFC) (OSA, 2020), pp. 1–3. Copyright 2020 Optical Society of America.

transmitting and receiving orthogonal beams that are composed of multiple LG modes, the performance of an LG-multiplexed link can be potentially improved.

## V. OAM MULTIPLEXING FOR FSO AIRBORNE COMMUNICATIONS

The communication capacity needs of manned and unmanned aerial platforms have been increasing dramatically over the past several years, thereby driving the need for higher-capacity links between these platforms and their ground stations.<sup>59–62</sup> OAM multiplexing techniques may be utilized to increase the data capacity and spectral efficiency and to reduce the probability of interception in FSO airborne communications.

### A. Challenges for OAM multiplexing for FSO airborne communications

As shown in Fig. 21, there are several scenarios in airborne and satellite FSO communications that require distinct applications and pose specific challenges including

- (i) *Satellite-to-satellite links* usually require ultra-long-distance beam propagation (>1000 km) and careful control over the laser beam divergence. In such a scenario, high sensitivity of the receiver detector is desirable since only a limited proportion of the transmitted beam can reach the receiver.<sup>63</sup> Ultralong links might also necessitate extremely large apertures due to the increased beam divergence of higher order modes.<sup>63</sup>
- (ii) *Satellite-to-ground-station links* generally utilize a laser beam to propagate through the Earth's atmosphere and the accumulated atmospheric turbulence effects would induce severe distortion on the wavefront of the optical beam.<sup>63</sup>
- (iii) *Airplane-to-ground links* involve a fast-moving airplane at a distance range of ~1 km–100 km. Both the optical beam

pointing/tracking and atmospheric turbulence effects are challenges in this scenario.<sup>64</sup>

- (iv) *UAV-to-ground-station communications*: a relatively slow-moving unmanned-aerial-vehicle (UAV) is hovering at a distance of <kilometer away from the ground station. UAVs have drawn a lot of attention over the recent years due to their potential for proliferating numerous applications.<sup>59,65–67</sup> In UAV-to-ground-station communications, distances may be relatively short range and a key challenge is to miniaturize the optical hardware.

In addition, these free-space applications share some common desirable characteristics, including (1) low size, weight, and power (SWaP), which can be alleviated by advances in integrated OAM devices,<sup>68</sup> and (2) accurate pointing, acquisition, and tracking (PAT) systems, which help limit modal coupling and crosstalk.<sup>30</sup>

### B. OAM-multiplexed communication links to and from UAV platforms

One example of the aerial platforms is the UAV, such as flying drones that are proliferating for numerous applications.<sup>59,65–67,69–71</sup> As the first example of OAM-multiplexed FSO airborne communications, an 80-Gbit/s OAM-multiplexed FSO link between a flying drone and a ground station was demonstrated.<sup>59</sup> As shown in Fig. 22, the ground station contained an OAM transmitter, an OAM receiver, and a beam tracking system. A retroreflector carried by the UAV was flown up to ~50 m away (i.e., ~100 m round trip) from the ground station to efficiently reflect the OAM beams that were emitted from the transmitter back to the receiver with little distortion.

As one example of misalignment issues, the effects of beam jitter on the system performance for OAM-multiplexed UAV platforms were evaluated.<sup>59</sup> In order to evaluate the effects of beam jitter, the statistics of the received beam centroid were measured. Figure 24 shows the relative positions of the beam when the UAV hovers in the air ~50 m relative to the ground station and ~10 m above the ground

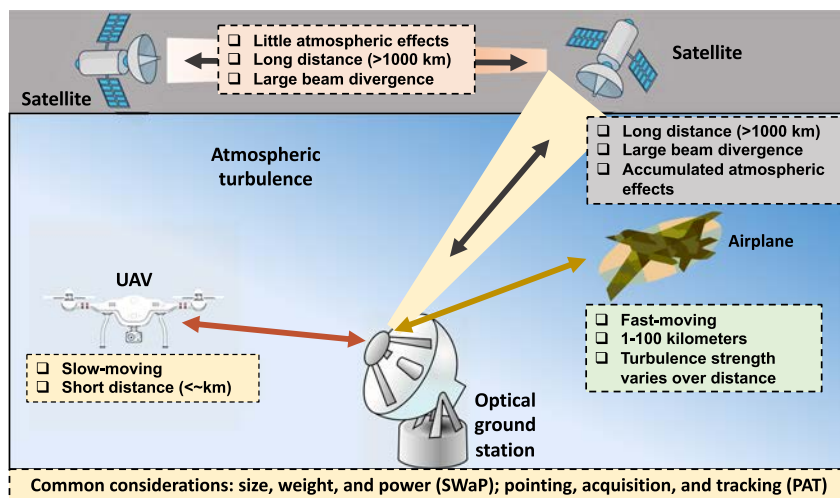


**FIG. 21.** OAM-multiplexed FSO airborne and satellite communications. The low size, weight, and power (SWaP) considerations can be alleviated by advances in the integrated OAM devices. The pointing, acquisition, and tracking (PAT) system requirements are determined by the key parameters of the FSO airborne links, such as the moving speed and link distance. Moreover, the turbulence effects can degrade the system performance for long-distance links in the atmosphere.



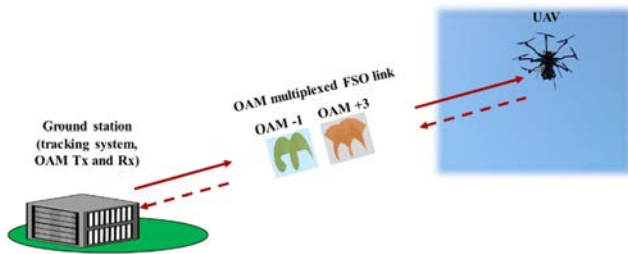


**FIG. 22.** Concept of an FSO communication link between a UAV and a ground station using OAM multiplexing. The ground station includes the tracking system as well as the OAM transmitter and receiver, and the UAV hovers in the air. Tx—transmitter and Rx—receiver. Reproduced with permission from Li *et al.*, Sci. Rep. 7, 17427 (2017). Copyright 2017 Macmillan Publishers.

with the tracking system on Fig. 23(a) and moves horizontally in the air at a speed of  $\sim 0.1$  m/s with the tracking system on Fig. 23(b), respectively. The OAM  $\ell = +3$  beam was transmitted. The statistics of each scenario were obtained by continuously capturing 1000 intensity profiles of the beam over a 120-s period using an infrared camera. The beam jitter variance was  $\sim 0.09$  mm<sup>2</sup> when the UAV was hovering and increased to  $\sim 0.46$  mm<sup>2</sup> when moving, respectively.

### C. MIMO for OAM-multiplexed UAV platforms under atmospheric turbulence effects

The atmospheric turbulence might not degrade much the performance of OAM-multiplexed UAV platforms under a clean weather condition and over a short distance. However, the effects of atmospheric turbulence would be more significant as transmission distances increase and weather conditions become worse. Due to the stronger distortion induced by the atmospheric turbulence, the received signal carried on a particular OAM mode may include larger power of signals leaked from other channels.

To mitigate atmospheric turbulence in UAV platforms, the MIMO equalization algorithm has been demonstrated to compensate for the inter-channel crosstalk.<sup>71</sup> A rotatable phase plate with a pseudo-random phase distribution was added to the 100-m UAV-to-ground link (the link presented in Fig. 22) to emulate the atmospheric turbulence. A  $4 \times 4$  adaptive MIMO equalizer

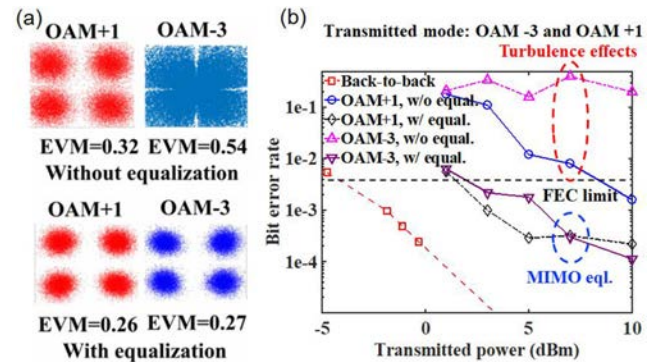


**FIG. 24.** (a) The measured QPSK constellation diagrams and corresponding EVMs for the OAM  $\ell = +3$  and  $\ell = -1$  beams without (upper line) and with (bottom line) the MIMO equalization. (b) Experimentally measured BERs for both channels as functions of transmitted power when the UAV was hovering  $\sim 50$  m away under turbulence without and with the MIMO equalization. Reproduced with permission from Zhang *et al.*, Opt. Lett. 44, 5181 (2019). Copyright 2019 Optical Society of America.

was implemented in a four-channel OAM multiplexed link and each channel carried 20-Gbit/s QPSK data. Figure 24(a) illustrates the measured 20-Gbit/s QPSK constellation diagrams and corresponding EVMs for the OAM  $\ell = +3$  and  $\ell = -1$  beams without and with the MIMO equalization. The MIMO equalization reduced the EVM from 32% to 54%–26% and 27% for the OAM  $\ell = +3$  and  $\ell = -1$  beams, respectively. Figure 24(b) shows BERs for both channels as functions of the transmitted power when the UAV was hovering with the phase plate fixed at a random angle. The experimental results indicate that MIMO equalization can help mitigate the crosstalk caused by turbulence and improve both the EVM and the BER of the signal in an OAM-multiplexed link for flying platforms.

### D. OAM beams for optical beam tracking

Beam tracking is considered important for a single-beam non-OAM FSO link, where misalignment between the transmitter and the receiver leads to an increase in power loss and BER.<sup>69,72</sup> For OAM-multiplexed UAV platforms, beam tracking might be even

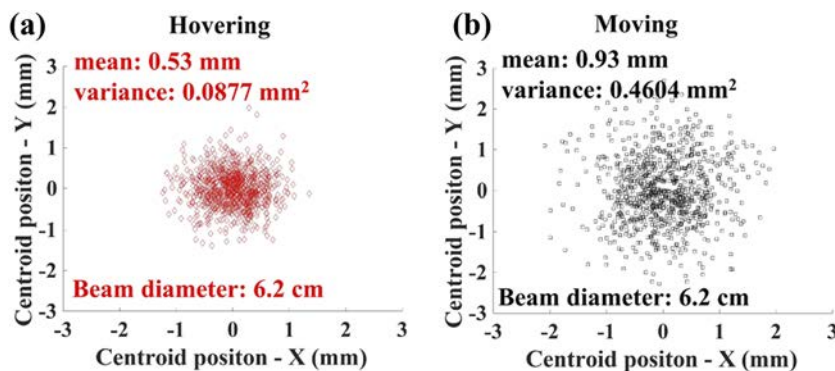


**FIG. 23.** Experimental results of beam jitter (OAM  $\ell = +3$  beam) in the flight environment: beam displacement with respect to the receiver center when the UAV is (a) hovering and (b) moving at a speed of  $\sim 0.1$  m/s, respectively. The UAV was at a distance of  $\sim 50$  m relative to the ground station and  $\sim 10$  m above the ground. Reproduced with permission from Li *et al.*, Sci. Rep. 7, 17427 (2017). Copyright 2017 Macmillan Publishers.

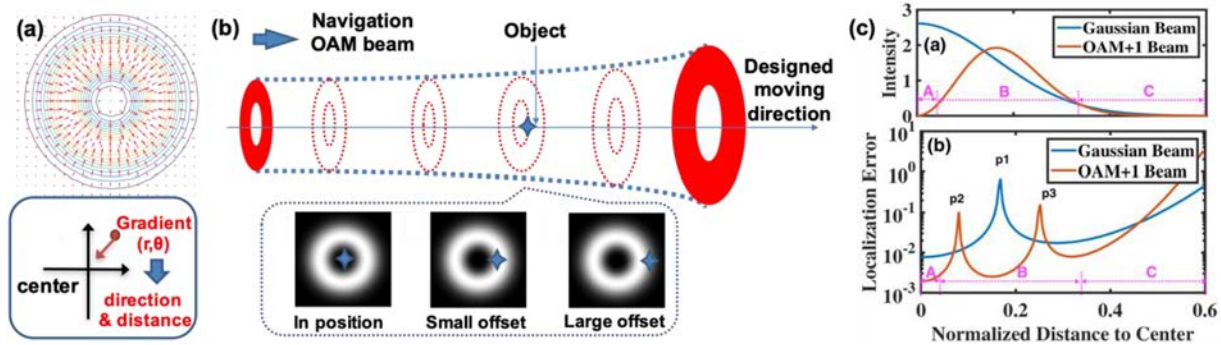


**FIG. 25.** Concept of utilizing an OAM beam for optical beam tracking: (a) The spatial gradient of an OAM beam as an error signal for beam tracking. (b) Concept of an OAM beam tracking and localization system. (c) Simulation results for the localization error by using the fundamental Gaussian beam and the OAM +1 beam. Reproduced with permission from Xie *et al.*, Opt. Lett. **42**, 395 (2017). Copyright 2017 Optical Society of America.

more important.<sup>59</sup> This is because the misalignment issue not only causes power loss but also power coupling among different OAM modes, thereby increasing the inter-channel crosstalk and BER. To maintain the precise alignment between the transmitter and the receiver, a pointing, acquisition, and tracking (PAT) system is typically used in UAV platforms.<sup>59</sup>

Beam tracking was demonstrated in single-beam non-OAM FSO links with or without using a probe beam at a separate wavelength.<sup>69,72</sup> Later on, beam tracking was also demonstrated in OAM-multiplexed FSO links using a Gaussian beacon. Such beam tracking systems typically utilize the displacement of the fundamental Gaussian beam as an error signal and utilize a fast-steering mirror (FSM) to correct the misalignment. As illustrated in Figs. 25(a) and 25(b), it has been proposed to use spatial gradient of an OAM beam as the error signal for beam tracking.<sup>73</sup> As presented in Fig. 25(c), when there is a displacement between the transmitter and receiver, the spatial gradient of an OAM beam can indicate the amount of displacement. Moreover, due to the unique phase and amplitude structure of an OAM beam, the spatial gradient of the OAM beams could potentially provide a low tracking error.

## VI. OAM MULTIPLEXING IN UNDERWATER ENVIRONMENT

There is a growing interest in high-capacity underwater wireless communication systems for supporting the significant increase in the demand for data, such as from sensor networks, unmanned underwater vehicles, and submarines.<sup>74</sup> Traditionally, acoustic waves have been used for underwater communications, but this technique has quite limited bandwidth capacity.<sup>75</sup> Alternatively, communication using optical frequencies in the low-attenuation blue-green region can enable higher-capacity underwater transmission links due to the much higher carrier-wave frequency.<sup>76</sup>

### A. Propagation effects in underwater environment

Blue-green light exhibits relatively low absorption in water, thereby potentially enabling high-capacity links with a distance of

~100 m.<sup>76</sup> Note that radio waves simply do not propagate well underwater, and common underwater acoustic links have a very low bit rate. As shown in Fig. 26, maritime and underwater environments pose various challenges, including loss, turbidity, scattering, currents, and turbulence. An interesting challenge is transmitting from above the water to below the water such that the structured optical beam would pass through inhomogeneous media surrounding the interface, including nonuniform aerosols above water, the dynamically changing geometry of the air-water interface, and bubbles/surf below the surface.<sup>77–82</sup>

There were several reports of propagation of OAM beams through turbid media that include water current and particle scattering effects.<sup>77,78</sup> For example, Fig. 27(a) shows the distorted intensity profiles of OAM beams affected by different environmental effects.<sup>78</sup> The effects of water current, scattering, and turbulence were

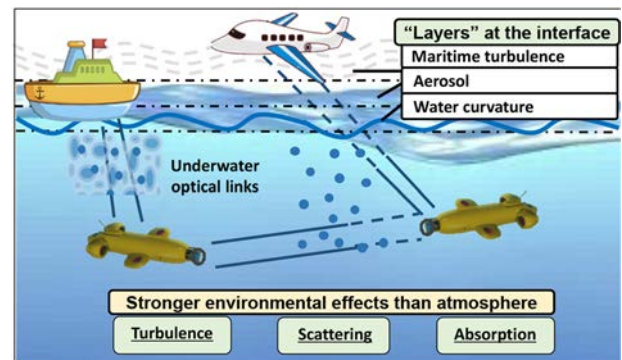


**FIG. 26.** Challenges in different scenarios for underwater FSO links. Environmental effects including turbulence (e.g., from water currents), scattering (e.g., from a turbid medium), and power loss due to water absorption are stronger than those in atmospheric environment. In addition, transmitting data from above the water to below the water could be an interesting challenge: the structured optical beam may pass through the inhomogeneous media surrounding the interface, including non-uniform aerosols above water, the dynamically changing geometry of the air-water interface, and bubbles/surf below the surface.

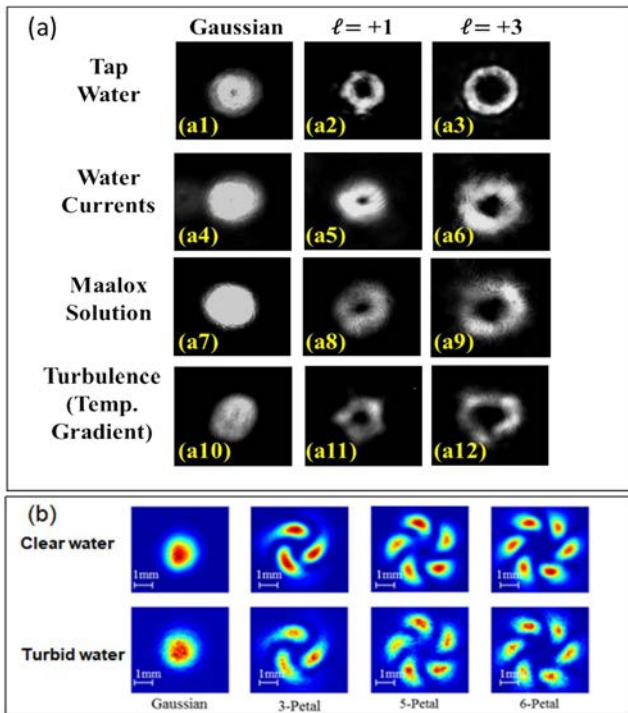


**FIG. 27.** (a) Measured intensity profiles of OAM beams under various channel degradation effects: [(a1)–(a3)] With only tap water, [(a4)–(a6)] with water currents, [(a7)–(a9)] with the Maalox solution, and [(a10)–(a12)] with thermal gradient-induced turbulence. (b) Experimentally measured intensity profiles for the combinations of concentric optical vortices after propagation in clear water (upper line) and turbid water (bottom line). Reproduced with permission from Ren *et al.*, *Sci. Rep.* 6, 33306 (2016). Copyright 2016 Nature Research. Reproduced with permission from Friedman, *The Naval Institute Guide to World Naval Weapon Systems* (Naval Institute Press, 2006). Copyright 2016 Naval Institute Press.

emulated by using circulation pumps, adding Maalox solution to water, and creating a thermal gradient by mixing cold/hot water. When OAM beams of  $\ell = +1$  and  $+3$  and a Gaussian beam were transmitted one at a time, the following were observed:

- In tap water:** the ring-shaped intensity profiles of the OAM beams tend to be maintained after  $\sim 1$ -m propagation and are slightly distorted by the water current.<sup>78</sup>
- With scattering:** there was a small time-varying change in the intensity profiles, which might be a result of the natural dynamic diffusive movement of the small particles contained in the water.<sup>78</sup>
- With water current or turbulence:** phase distortion became stronger such that the phase front of the OAM beam was distorted.<sup>78</sup>

Besides the transmission of a single vortex beam, another work explored the utilization of spatial profiles generated by the coherent combination of multiple concentric optical vortices in the underwater environment.<sup>74</sup> This approach provides an alternative way for utilizing OAM modes in the underwater environment. The intensity profiles of the combinations of concentric optical vortices are

presented in Fig. 27(b). Due to the interference between concentric vortices, the resulting beam has a periodic constructive and destructive interference around the center of the beam, i.e., a “petal” pattern. The results show that the “petal” pattern experiences little distortion when the beams propagate through clear water. However, after propagating through turbid water, the intensity profiles of the beams are distorted due to the scattering effects.

## B. OAM-multiplexed links in underwater environment

In the previous session, we describe propagation effects of OAM-carrying beams in underwater environment. We will present examples of OAM-multiplexed communication links in the underwater environment considering the above-discussed effects in this session. For underwater environments, there have been several reports on blue-green light non-OAM links with a single-beam and a distance of  $\sim 100$  m.<sup>76</sup> To further increase the data capacity in underwater environment, blue-green light OAM-multiplexed links were demonstrated over a few meters in an emulated underwater environment.<sup>77,78,82</sup> A direct way to modulate a blue-green light is to use an internal modulation. For example, by directly modulating the driving current of a 520 nm laser diode, a 1-Gbit/s signal was produced.<sup>78</sup> However, due to the limited bandwidth of the internal modulation of the commercially available laser diodes, the maximal data rate of the green beam was  $\sim 1$  Gbit/s. To achieve larger data rates in underwater environment, a high-speed modulated light at a lower frequency can be wavelength converted to blue-green light by second harmonic generation. For example, by using a 10-Gbit/s 1064-nm lithium niobate modulator and a frequency-doubling module, a 10-Gbit/s signal was generated, and the carrier wavelength was converted from 1064 nm to 532 nm.<sup>78</sup>

Figure 28 presents the average BER of the channels on the OAM  $+1$  and  $+3$  beams with and without equalization, with each OAM beams carrying a 10-Gbit/s on-off keying signal.<sup>78</sup> To mitigate the thermal-gradient-induced crosstalk in water, the constant modulus algorithm (CMA) equalization is implemented in the DSP.

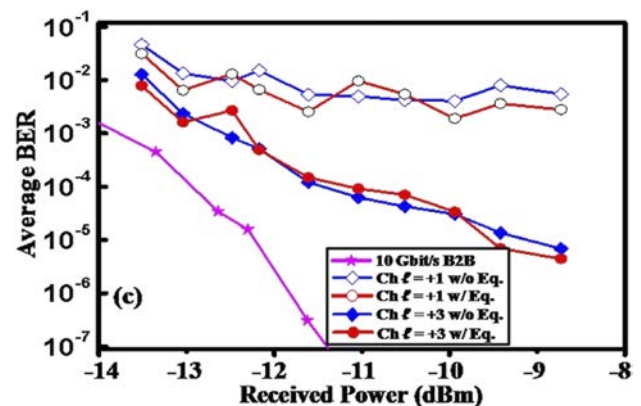


**FIG. 28.** Experimental results: BER curves of OAM channel  $\ell = +1$  and  $\ell = +3$  with and without CMA equalization—each OAM beam carries a 10-Gbit/s on-off keying signal. Thermally induced refractive index inhomogeneity in water causes the BER to reach an error floor. With CMA equalization, BERs improve significantly and are below the FEC limit. Ch—channel. Eq.—equalization. Reproduced with permission from Ren *et al.*, *Sci. Rep.* 6, 33306 (2016). Copyright 2016 Nature Research.



The measured BERs were averaged over 1 min of data for two OAM channels ( $\ell = +1$  and  $+3$ ) before and after applying the CMA equalization. Due to inter-channel crosstalk, the measured BER curves without  $2 \times 2$  equalization reached a BER error floor. With the CMA equalization, the BER performance is improved and could reach below the forward error correction (FEC) limit.<sup>78</sup> We note that the FEC limit is a BER upper limit under which the FEC method can be performed when coding the channel that can control the errors over unreliable or noisy communication channels.

## VII. NOVEL BEAMS

This section is for the completeness of this review paper besides the discussions for free-space communications. The excitement in the field of novel beams originated by the ability to utilize orthogonal structured optical beams. However, there is much work in the fields of optics and photonics on several types of novel variations of optical beams (e.g., Airy and Bessel types), with more being explored at an exciting pace.

Over the next several years, it would not be surprising if novel beams are used to minimize certain system degrading effects. There have been initial results for some of these concepts, but a partial “wish list” for novel beams could be beams

- (i) that are more resilient to the modal coupling caused by turbulence and turbidity,
- (ii) that have limited divergence in free space,
- (iii) that are resilient to partial obstruction such that their phase structure can “self-heal” (e.g., Bessel-type beams), and
- (iv) whose phase structure can readily be recovered even if the transmitter and receiver are misaligned.

Generally, FSO communication links rely on the line-of-sight (LOS) operation, and thus, the obstructions in the beam path are one of the potential challenges. In particular, for OAM communication links that are partially blocked, an OAM beam will produce distortions in its beam profile. This will reduce the orthogonality between the different OAM beams and cause power coupling from the desired OAM mode to neighboring OAM modes, thereby leading to signal fading and channel crosstalk. As one example,

Bessel–Gaussian (BG) beams have displayed the unique property to reconstruct or “self-heal” the transverse intensity and phase profiles after experiencing an obstruction. The self-healing property of BG beams is due to the delocalized transport of the beam energy and momentum, which can replace the scattered light by the obstructions.<sup>83</sup> As another example of novel beams, the Airy beam has unique properties, including being non-diffracting, self-bending, and self-healing.<sup>84</sup> Due to its curved parabolic trajectory, the Airy beam has been demonstrated to be able to circumvent obstacles in an FSO interconnection link.<sup>85–87</sup>

As one example of approximations to true Bessel beams, BG beams are non-diffractive and self-healing over a limited Bessel-range. The self-healing property of the BG beams was utilized to mitigate the degrading effect due to obstruction in short-range FSO OAM communication links.<sup>88</sup> As shown in Fig. 29(a),  $N$  OAM beams, each carrying a distinct data channel, are spatially multiplexed and transmitted through an axicon to be transformed into BG beams. Within the Bessel region, the beams are propagation invariant and, therefore, can sustain partial obstructions. At the end of the Bessel region, an exit axicon that has opposite cone angles is placed to remove the conical phases. Finally, an OAM mode demultiplexer separates each OAM beam. In the experiment, two OAM-multiplexed channels (OAM  $l = +1$  and  $l = +3$ ) each carrying 100-Gbit/s QPSK signals were transmitted through a path with obstructions.<sup>88</sup> As an example, the transverse intensity profiles of the obstructed and unobstructed BG beam with  $l = +3$  are presented in Fig. 29(b). An obstruction was placed at the beam center, and images of the transverse intensity profiles were taken at various locations along the propagation direction. A comparison between the obstructed and unobstructed beams in the plane of the demultiplexer revealed the self-healing property of the BG beam. Figure 29(c) illustrates the BER measurement for the unobstructed and obstructed BG beams. Both channels achieve BERs below the FEC limit.

## VIII. UTILIZING OAM IN QUANTUM SYSTEMS

In the case of a quantum communication system, an individual photon can carry one of many different OAM values; this is

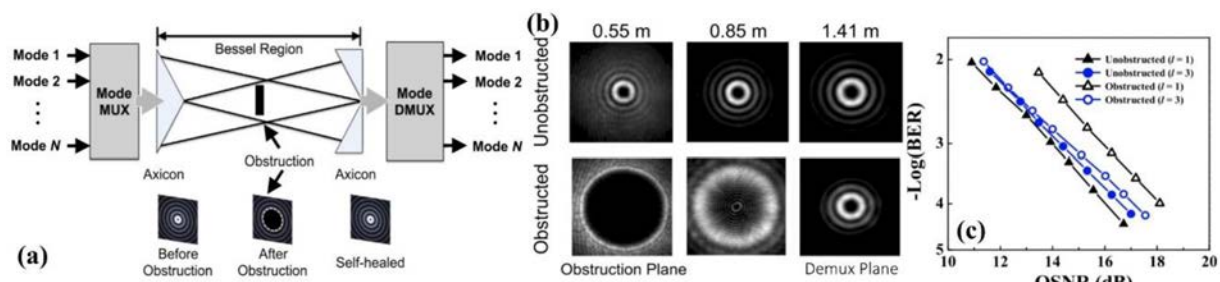


**FIG. 29.** (a) Conceptual diagram of an MDM link using multiplexed Bessel–Gaussian (BG) beams. The “Bessel-region” is the distance over which BG beams are propagation invariant and retain their profile. The insets depict the transverse intensity profiles of a BG beam before and after being obstructed by an opaque disk and in the receiver plane. (b) Measured transverse intensity profiles of the obstructed and unobstructed BG beam  $l = +3$  after an obstruction of radius 1.5 mm at different locations along the propagation direction. (c) Measured BER for the multiplexed BG beams obstructed by obstructions of radii  $r_{\text{obs}} = 1$  mm. Reproduced with permission from Ren *et al.*, Sci. Rep. 6, 33306 (2016). Copyright 2016 Nature Research.

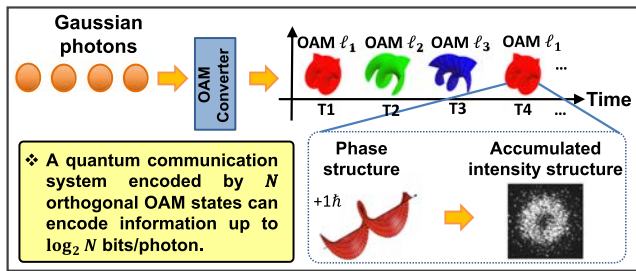


**FIG. 30.** Concept of OAM-based quantum data encoding. Within each symbol period, a Gaussian photon is converted to one of the  $M$  OAM states, resulting in information encoding of up to  $\log_2 M$  bit/photon. The accumulated intensity structure image is recorded using a single-photon-sensitivity low-noise intensified charge coupled device camera.<sup>89</sup>

similar to digital data taking on one of many different amplitude values and enables OAM-based encoding in quantum systems. If each photon can be encoded with a specific OAM value from  $M$  possibilities, the photon efficiency in bits/photon can be increased. This has the potential to be quite useful for quantum communication systems, which are typically photon “starved” and for which qubits can commonly be encoded on one of the only two orthogonal polarization states.<sup>89–93</sup> Figure 30 presents the concept of the OAM-based quantum encoding. Using an OAM mode converter, within each symbol period, the coming single Gaussian photon is converted to the respective OAM photon and occupies one of the  $M$  OAM states. Each photon has a helical phase front after being processed by the OAM converter. The accumulated intensity structure indicates that it has a ring-like intensity probability distribution.<sup>89</sup>

A larger alphabet for each qubit is, in general, highly desirable for enhancing the system performance. However, there is much research needed to overcome the challenges in fielding an OAM-encoded quantum communication system, such as (i) mitigating coupling among orthogonal states and (ii) developing transmitters that can be tuned rapidly to encode each photon on one of many modes.

### A. AO for quantum OAM encoding systems

Similar to OAM based classical FSO communication links, the system performance degradation due to the atmospheric turbulence

is a key challenge also for OAM-based quantum FSO links. Turbulence affects the phase front of the photon and thereby increases the intermodal crosstalk in the quantum communication system.

In order to mitigate the turbulence effect, the AO approach can be applied to OAM-encoded quantum communication links by using a classical Gaussian probe beam (i.e., OAM  $\ell = 0$ ) for the phase detection on a wavefront sensor. As shown in Fig. 31, the AO approach was demonstrated for the compensation of emulated turbulence in an OAM-encoded FSO quantum communication link at a transmitted rate of 10 Mbit/s.<sup>92</sup> The quantum channel and the classical Gaussian probe beam propagate coaxially through the emulated atmospheric turbulence. Using the distortion information gathered from the classical Gaussian probe beam, the AO system compensates the turbulence effects on the received channel and mitigates the distortion on the OAM-carrying photons. Due to the large power difference between the quantum channel and the classical probe beam (the power of the quantum channel is  $\sim 100$  dB lower than that of the classical probe beam), one may need to transmit the probe beam with different polarization, wavelengths, and OAM orders compared to the quantum channel in order to efficiently separate the classical probe beam from the quantum channel at the receiver side.

Figure 32 shows the channel transfer matrices (top panels) when sending OAM modes  $\{\ell = -3, \dots, +3\}$  one by one, as well as the photon count ratio (bottom figures) on the received OAM modes (i.e., the ratio of the received photons on the desired OAM modes to the total received photons) when sending only OAM  $\ell = 1$  photons in different cases: (from left to right) the back-to-back link (i) without probe and (ii) with the probe under atmospheric turbulence distortion, (iii) without probe, and (iv) with the probe and without AO mitigation, and (v) with the probe and with AO mitigation. Turbulence-induced distortion to the wavefront of OAM-carrying photons increases the probability of OAM photons existing in the undesired orders. Photons are better confined to their desired OAM orders with AO mitigation.<sup>92</sup>

### B. OAM-based quantum key distribution

Quantum cryptography, such as the quantum key distribution (QKD), can be utilized to build secure communication links between many parties. There have been reports of the demonstration of such systems in polarization-based optical systems.<sup>94–97</sup>

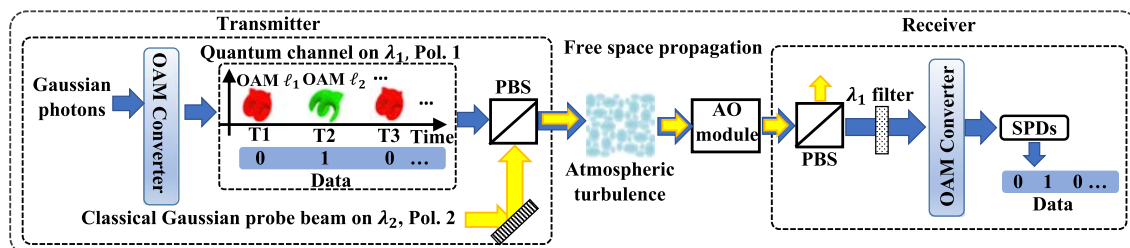


**FIG. 31.** The concept diagram of an OAM-encoded FSO quantum communication link through atmospheric turbulence with AO compensation. A classical Gaussian probe beam is transmitted coaxially with the quantum channel for the phase detection in the AO module. The probe beam and the quantum channel have different wavelengths, polarization, and OAM orders for the efficient separation at the receiver side. SPD—single photon detector, Pol.—polarization, AO—adaptive optics, and PBS—polarizing beam splitter.

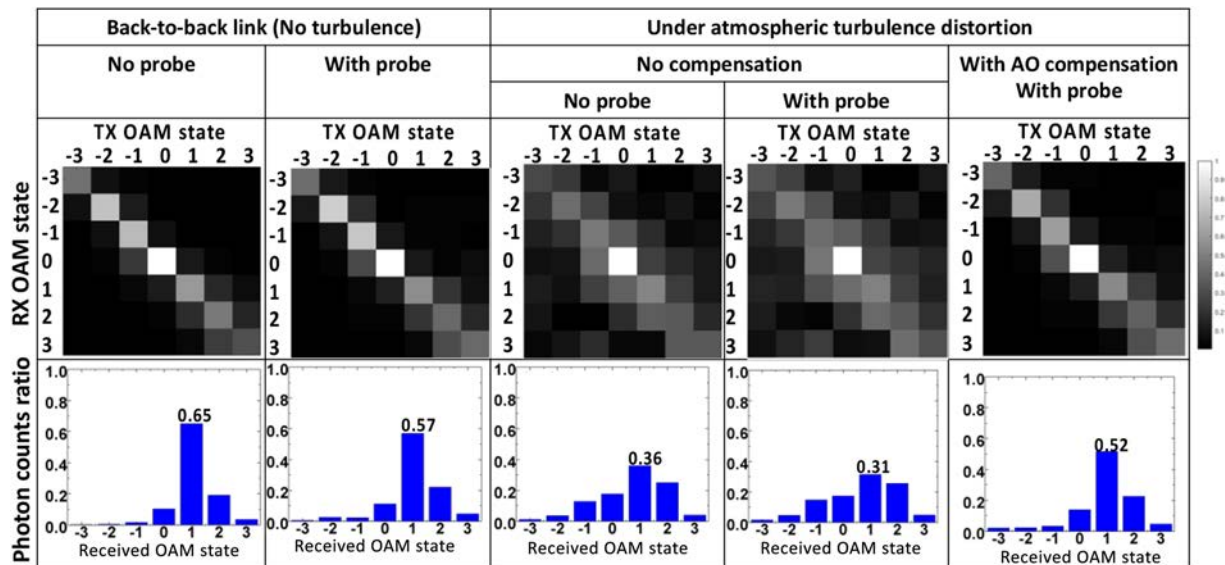


**FIG. 32.** Experimental results: the performance of AO mitigation in an OAM-based quantum link. Upper line: channel transfer matrices when sending OAM modes  $\{\ell = -3, \dots, +3\}$ , respectively, for different cases. The numbers are measured in the quantum domain as the ratio of the measured photon counts to the maximum photon counts in this matrix in the unit of dB. Lower line: the photon counts ratio on received OAM modes  $\{\ell = -3, \dots, +3\}$  when sending only OAM  $\ell = 1$  photons for different cases. TX—transmitter and RX—receiver. Reproduced with permission from Liu *et al.*, Research **2019**, 8326701 (2019). Copyright 2019 American Association for the Advancement of Science.

As another degree of freedom, the OAM state of the light has the potential to enable QKD schemes using a higher-dimensional encoding scheme.<sup>98–101</sup> Figure 33(a) presents the concept of utilizing high-dimensional OAM-based QKD in a  $\sim 300$ -m FSO quantum communication link.<sup>102</sup> Two sets of mutually unbiased bases (MUBs) including two vector modes and two OAM modes were combined to form four-dimensional quantum states. The transmitter part consists of a single-photon source and the setup of Alice (i.e., transmitter) to prepare states. The receiver part consists of the

single-photon detection system and Bob's (i.e., receiver) setup to measure the states. A two- or four-dimensional BB84 protocol was performed under different atmospheric conditions exhibiting moderate turbulence effects. Specifically, Alice prepares the signal photon in one of the MUB states using an appropriate sequence of wave plates and q-plates and combines these with idles photons using a polarization beam splitter (PBS) and spatially magnifies the beams. Bob used a mirrored sequence of wave plates, PBSs, lenses, and q-plates and measured the signal photon by projecting the

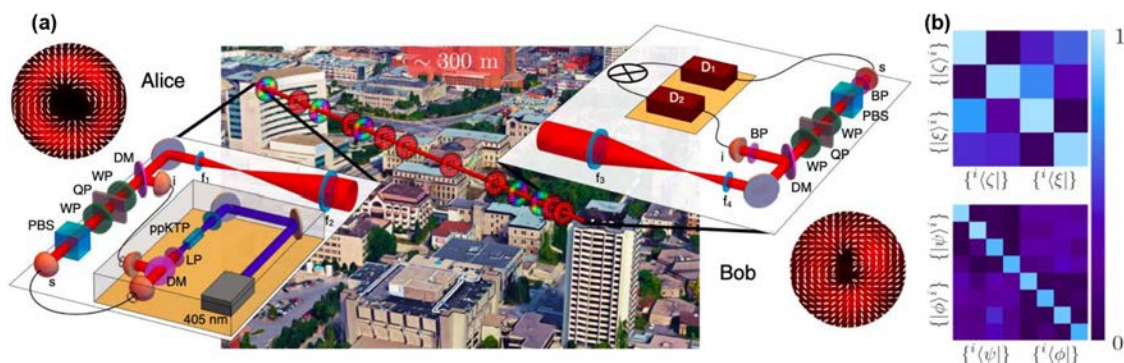


**FIG. 33.** The 300-m intracity quantum communication link in Ottawa. (a) The schematic diagram of the sender (left) with a single-photon source and Alice's quantum state preparation setup. Alice prepares a state from the OAM modal set or vector modal set using a polarization beam splitter (PBS), wave plates (WP), and a q-plate (QP). Bob, the receiver (right), can perform measurements on the sent states and record the coincidences between the signal and idler photons with detectors  $D_1$  and  $D_2$  in a coincidence logic box. (b) The measured probability-of-detection matrices give quantum bit error rates of 5% and 11% for two and four dimensions, respectively. Reproduced with permission from Sit *et al.*, Optica **4**, 1006 (2017). Copyright 2017 Optical Society of America.



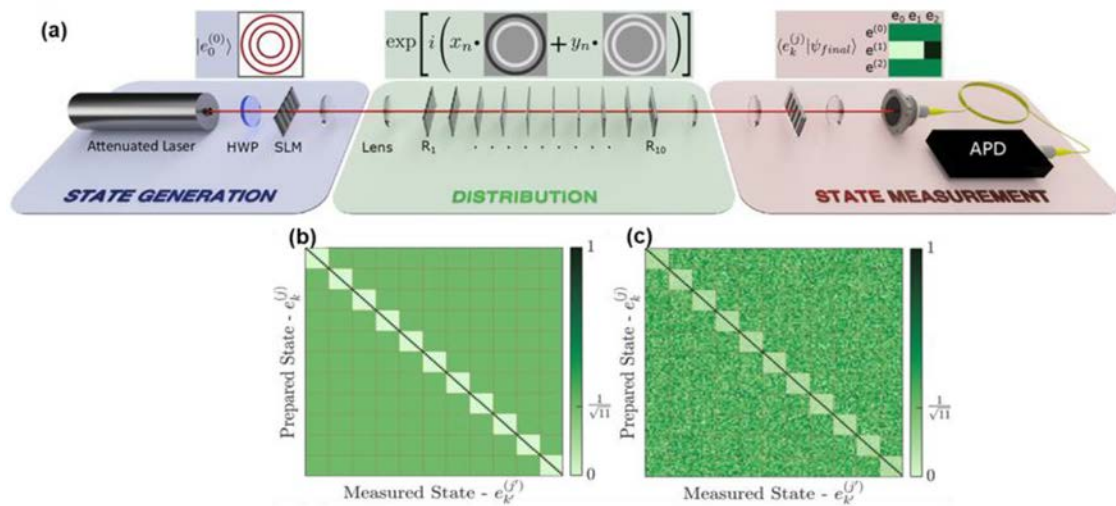


**FIG. 34.** (a) Conceptual approach for quantum secret sharing using perfect vortex beams illustrated for dimension  $d = 3$ . The distributor generates a photon that comprises  $d$  number of concentric rings, with each having a different OAM value. Every participant applies their unitary transformation. The final participant transmits the qudit state back to the distributor who measures the state in the  $j$ th mutually unbiased bases, obtaining the outcome showing here as a probabilistic mode projection measurement. (b) Simulated and (c) experimentally measured  $11^2 \times 11^2$  detection probability matrix for a high-dimensional quantum secret sharing experiment using 11 OAM states.<sup>106</sup> Reproduced with permission from Pinnell *et al.*, *Laser Photonics Rev.* **14**, 2000012 (2020). Copyright 2020 Wiley.

photon onto one of the states from one of the MUBs.<sup>102</sup> To optimally detect the signal photon, Bob should project onto the same state that Alice sent. Probability-of-detection matrices for the quantum states [Fig. 33(b)] give quantum-bit-error rates (QBERs) of 5% and 11% in the two- and four-dimensional protocols, respectively, which are below the respective security thresholds.

In typical QKD schemes, a classical key is shared between the two parties.<sup>94</sup> In the past decade, schemes for generating correlated classical keys shared among multiple parties were developed, namely, the quantum secret sharing (QSS) protocols.<sup>103</sup> The most common candidate for the experimental implementation of single photon QSS schemes is based on the polarization of light (two dimensions).<sup>104,105</sup> A recent work demonstrated a proof-of-concept implementation of a QSS scheme using OAM states with a dimension of 11.<sup>106</sup> As shown in Fig. 34(a), a distributor generates a photon that is a combination of 11 OAM states. Every participant applies their unitary transformation. The final participant sends the qudit state back to the distributor who measures the state. The distributor's secret can be determined through the collaboration of the remaining participants. The detected 11-dimensional probability matrix results in Figs. 34(b) and 34(c) indicate that OAM states offer a higher dimensionality and can be utilized for high-dimensional quantum information processes.<sup>106</sup>

## IX. OAM MULTIPLEXING IN RF, mm-WAVE, AND THz REGIMES

Besides using optical beams, free-space communication links can take advantage of mode multiplexing in many other carrier-wave-frequency ranges to increase the system capacity. For example,

OAM can manifest in various types of electromagnetic and mechanical waves, and interesting studies have explored the use of OAM in radio frequency, millimeter, acoustic, and THz waves,<sup>8,107–118</sup> as shown in Fig. 35. From a system designer's perspective, there tends to be a trade-off in different frequency ranges:

- Divergence:** lower frequencies have much higher beam divergence, which makes it more challenging to collect enough power of the beam to recover the data channels.
- Interaction with matter:** lower frequencies tend to have much lower interaction with matter such that radio waves

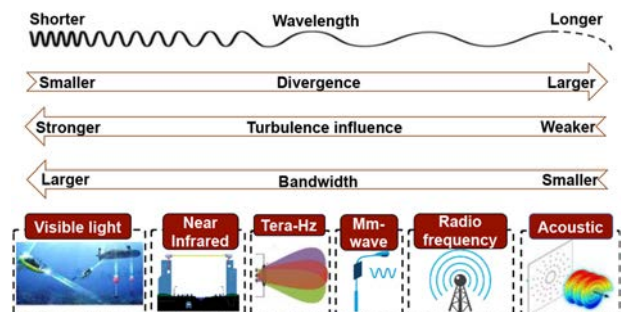


**FIG. 35.** OAM multiplexing for communications using different carrier-wave frequencies. The orthogonality among different OAM beams does not change with the carrier-wave frequency. Thus, OAM multiplexing can be utilized for any electromagnetic (EM)-wave communication link. EM OAM waves of different wavelengths interact with matters (e.g., propagation media) differently and have different divergence.

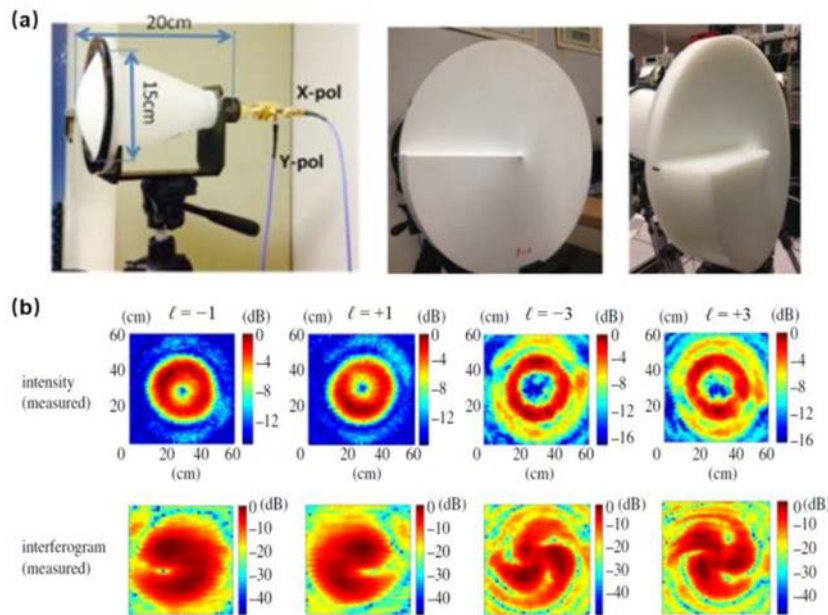


**FIG. 36.** A 32-Gbit/s data transmission at a 28 GHz carrier frequency by multiplexing four OAM modes and two polarizations.<sup>8</sup> (a) Left to right: horn antenna, SPP for OAM +1, and SPP for OAM +3 for generating RF OAM beams. (b) Measured intensity profiles of generated OAM beams and their interferograms. SPP: spiral phase plate. Reproduced with permission from Yan *et al.*, Nat. Commun. 5, 4876 (2014). Copyright 2014 Macmillan Publishers.

are less affected by atmospheric turbulence induced modal coupling than optical waves.

### A. OAM-multiplexed links in RF and mm-wave regimes

OAM can be carried by any EM wave with a helical wavefront, and this does not depend on the carrier-wave frequency. Therefore, OAM multiplexing for communications can be applied to the RF regime. The feasibility of using OAM beams to increase the system capacity and the spectral efficiency of LOS RF communications is being actively investigated.<sup>8,108–113</sup>

There are exciting developments in the RF and mm-wave OAM application space, and industrial labs are increasingly engaging in R&D to significantly increase the potential capacity of fronthaul and backhaul links.<sup>8,108–113</sup> One proof-of-concept demonstration presented a 32-Gbit/s OAM-multiplexed link containing four OAM modes and two polarizations at a carrier-wave frequency of 28 GHz.<sup>8</sup> As shown in Fig. 36, four different OAM beams with  $l = -3, -1, +1, +3$  on each of the two polarizations were generated using spiral phase plates (SPPs) made from high-density polyethylene. Figure 36(a) shows the horn antenna, SPP for OAM +1, and SPP for OAM +3 at the frequency of 28 GHz. Figure 36(b) presents the observed intensity profiles for each of the beams and their interferograms with a Gaussian beam. After spatial combining using specially designed beam splitters, the resulting eight multiplexed OAM beams propagated for a distance of  $\sim 2.5$  m and were separated at the receiver. All eight OAM channels, each carrying a 4-Gbit/s 16-QAM signal, were sequentially recovered, achieving a capacity of 32 Gbit/s and a spectral efficiency of  $\sim 16$  bit/s/Hz.

The demand for larger bandwidth has gained much interest in OAM-multiplexed links at higher carrier frequencies using

different types of OAM generators/receivers.<sup>113,116–124</sup> For example, a 32-Gbit/s wireless link using OAM and polarization multiplexing was demonstrated at a carrier frequency of 60 GHz.<sup>120</sup> Advances in OAM generators/receivers for higher carrier frequencies include the use of RF antenna arrays that are fabricated on printed-circuit boards (PCBs).<sup>112</sup> For example, a multiantenna element ring can emit a mm-wave OAM beam by selectively exciting different antenna elements with a differential phase delay.<sup>113</sup> This is shown in Fig. 37(a), where the antenna arrays use delay lines of different lengths to set the phase of each patch antenna element in order to generate OAM beams of different orders. Moreover, the concept could be extended to multiplex  $N$  OAM beams. Multiple concentric rings can be fabricated, resulting in a larger number of

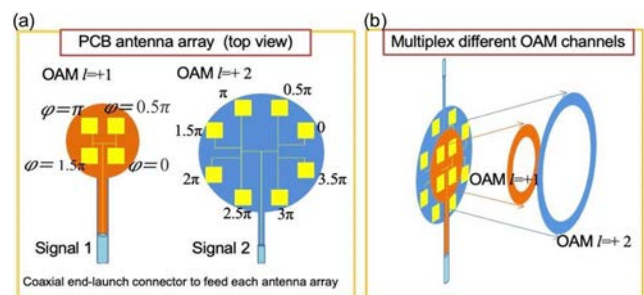


**FIG. 37.** Concept of using multi-layer patch antenna arrays to multiplex multiple OAM modes. (a) Top view of the stacked patch antenna fabricated on printed-circuit boards (PCBs). (b) Multiple antenna array layers are fed by independent data streams for OAM multiplexing. Reproduced with permission from Zhao *et al.*, 2016 IEEE International Conference on Communications (ICC) (IEEE, 2016), pp. 1–6. Copyright 2016 IEEE.





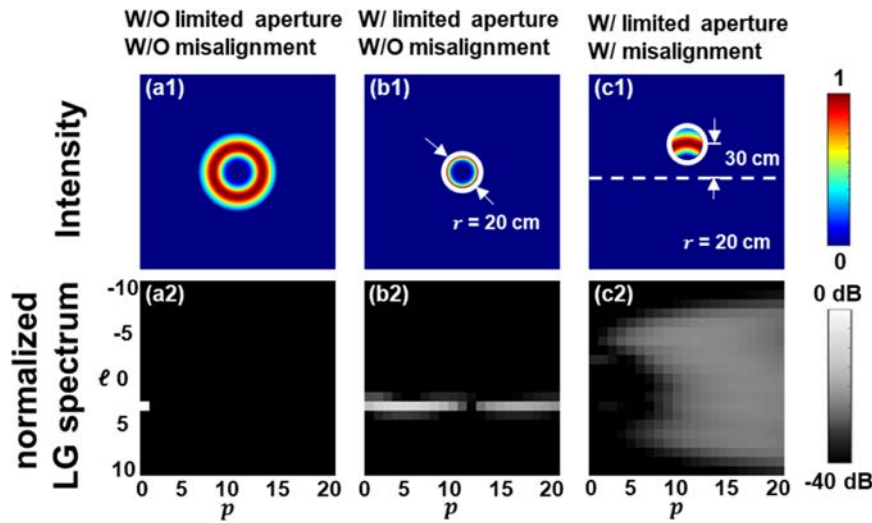


**FIG. 39.** Simulation results: intensity profiles and normalized 2D LG spectra of THz OAM beams (a) without the influence of limited aperture size or misalignment, (b) with a limited aperture size of 20 cm in radius, and (c) with a limited aperture size of 20-cm radius and a 30-cm misalignment when transmitting OAM +3 with the beam waist  $w_0 = 5$  cm through a 40-m link. A limited-size aperture would induce modal power coupling to high-order  $p$  modes, and misalignment would induce modal power coupling to both neighboring  $\ell$  and  $p$  modes. Reproduced with permission from Su *et al.*, 2020 IEEE Globecom Workshops (GC Wkshps) (IEEE, 2020), pp. 1–6. Copyright 2020 IEEE.

arrays (16 antennas/array) for OAM generation and a single antenna at the center. Each UCA can concurrently transmit or receive five OAM mode signals ( $0, \pm 1, \pm 2$ ) carrying five independent data streams.<sup>129</sup> Thus, the UCAs could support the transmission of 21 data streams in total. At the receiver, other UCAs were utilized

to select different OAM modes and receive the multiplexed data channels. Combinations of 16-QAM and 64-QAM with various low-density parity check channel coding rates for FEC successfully yielded a 100-Gbit/s data rate in a wireless communication link over a distance of 10 m, and the setup is shown in Fig. 42(b). Moreover,

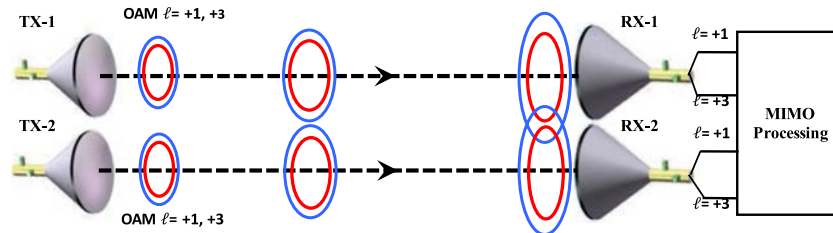


**FIG. 40.** Concept of a LOS mm-wave communications link that employs OAM multiplexing over conventional spatial multiplexing. The system consists of two transmitter/receiver apertures, with each transmitter aperture containing two OAM modes. At the receiver, Rx-1(or Rx-2) could receive power from all four OAM modes from the two transmitters, where the power from the two OAM modes transmitted from Tx-2 (or Tx-1) induces crosstalk. Tx—transmitter. Rx—receiver. Reproduced with permission from Ren *et al.*, IEEE Trans. Wirel. Commun. **16**, 3151 (2017). Copyright 2017 IEEE.

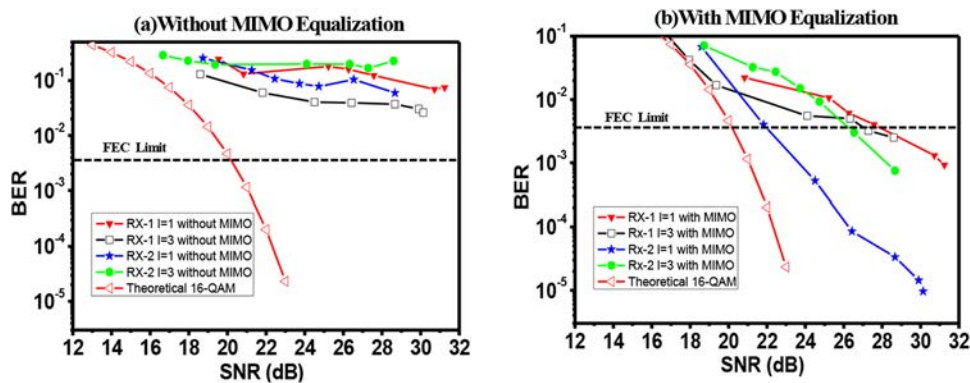


**FIG. 41.** BER measurements of OAM and MIMO communications (a) without MIMO—BERs are all above the FEC limit, exhibiting the error-floor phenomenon—and (b) with MIMO—BERs for all four OAM channels decreased to be below the FEC limit. Reproduced with permission from Ren *et al.*, IEEE Trans. Wirel. Commun. **16**, 3151 (2017). Copyright 2017 IEEE.

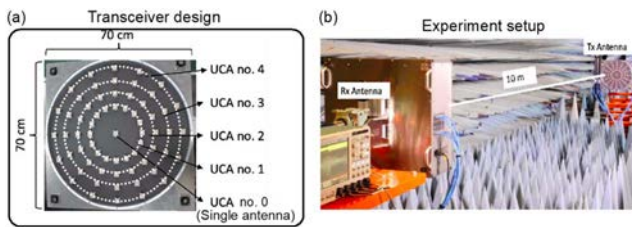


**FIG. 42.** (a) The structure of multiple concentric uniform circular antenna (UCA) arrays, with each array transmitting and receiving five OAM modes. (b) Experimental setup of a 10-m link using the combination of OAM multiplexing and conventional spatial multiplexing. Reproduced with permission from Sasaki *et al.*, 2018 IEEE Global Communications Conference (GLOBECOM) (IEEE, 2018), pp. 1–6. Copyright IEEE 2018.

a more recent work reported a 100-Gbit/s 100-m link by combining OAM multiplexing and polarization multiplexing at the 40 GHz frequency band.<sup>130</sup>

## X. OAM IN FIBER

This section is for the completeness of this review paper besides the discussions for free-space communications. MDM can be implemented in both free-space and fiber, with much of the transmitter and receiver technology being similar. However, the channel medium is different, which gives rise to the following distinctions:

- (i) There is no beam divergence in a light-guiding fiber.

- (ii) Fiber has inhomogeneities, and coupling can occur among modes, either within a single mode group or between different mode groups, thereby creating deleterious inter-channel crosstalk.<sup>5,131,132</sup>

The excitement around using MDM for capacity increase originally occurred primarily in the fiber transmission world, especially in research laboratories.<sup>16,19,133–138</sup> There were several reports of using linearly polarized (LP) modes as the modal set in fiber. However, since there was significant modal crosstalk when propagating through conventional-central-core few-mode fiber (FMF), MIMO-like DSP was used with impressive results to mitigate crosstalk.<sup>133,134</sup> It should be noted that modal basis sets can typically be represented by a modal combination of other sets. Therefore, it is no surprise that OAM and HG modes have also been used in conventional-type fibers, but significant crosstalk still occurs.

OAM has also been used as the modal basis set for fiber transmission for both central-core and ring-core FMFs.<sup>5,16,20,135</sup> Importantly, the modal coupling itself can be reduced in the optical domain by utilizing specialty fiber that makes the propagation constants of different modes quite different, thus reducing intermodal coupling. Such fibers include ring-core and elliptical-core fiber,<sup>20,135,139</sup> and tens of modes with low crosstalk have been demonstrated. These specialty fibers have produced exciting results, but they are structurally different than conventional fiber and thus require a little more resolve in order for them to be widely adopted. One design of the vortex fiber is shown in Fig. 43 as an example.<sup>68</sup> This vortex fiber has an annular refractive

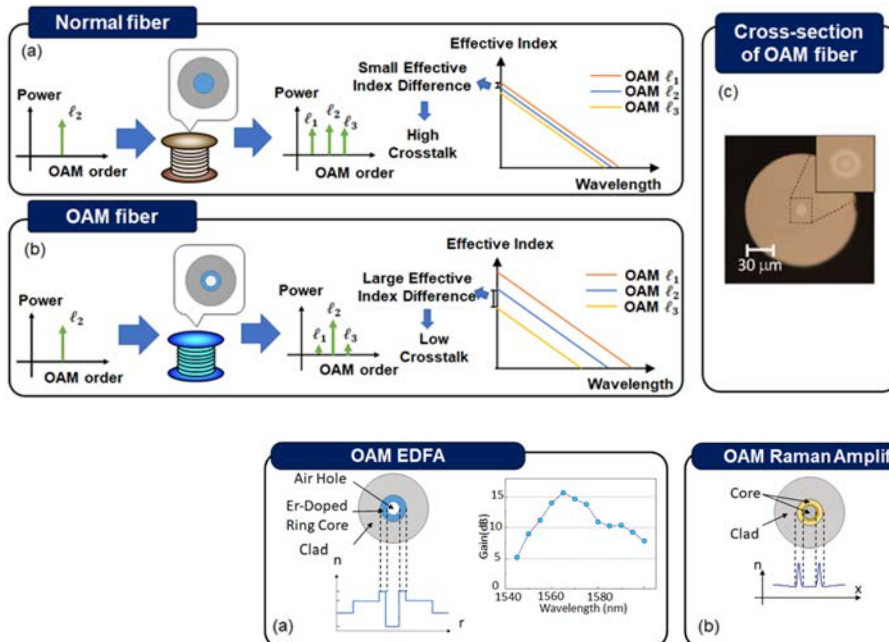


**FIG. 43.** (a) and (b) Comparison between (a) the normal fiber and (b) the vortex fiber. The OAM fiber has an annular refractive index profile, leading to a large effective refractive index difference among different OAM modes. Thus, the modal coupling is small during OAM beams' propagation in the special fiber. (c) The cross section of OAM fiber. Reproduced with permission from Bozinovic *et al.*, Science **340**, 1545 (2013). Copyright 2013 AAAS.

**FIG. 44.** Two examples of OAM fiber amplifiers. (a) The OAM EDFA has a higher gain, but it is hard to provide a flat gain over a broad bandwidth. (b) The OAM Raman amplifier has a lower gain with a flatter curve over ~30 nm. EDFA: Erbium-Doped Fiber Amplifier. Reproduced with permission from Jung *et al.*, J. Light. Technol. **35**, 430 (2017). Copyright 2017 Optical Society of America. Reproduced with permission from Zhu *et al.*, 2018 Optical Fiber Communication Conference (OSA, 2018), Paper W4C.4. Copyright 2018 Optical Society of America.

index profile to provide a large effective refractive index difference among different OAM modes as compared to a normal fiber. Thus, this vortex fiber design could potentially enable the efficient co-propagation and (de)multiplexing of OAM modes with lower inter-modal crosstalk.<sup>16,135</sup>

Another challenge for achieving MDM in fiber is the power loss due to fiber attenuation, which limits the transmission distance. In general, fiber-based amplifiers can be utilized to increase the transmission distance. For an MDM system, two main features are desired for the amplifiers: large mode gain and small difference between gains over different modes. Figure 44 presents two examples of OAM fiber amplifiers to address the above features. By using the ring-core fiber structure, OAM erbium-doped fiber amplifiers (EDFA)<sup>140,141</sup> and Raman amplifiers<sup>142</sup> have been demonstrated in these two papers, respectively. As for the performance, the example of OAM EDFA provides a high gain of >10 dB over a bandwidth of 20 nm, while the gain curve is not flat. As a comparison, the example of the OAM Raman amplifier has a low gain of ~3 dB with a flat gain curve over a bandwidth of 30 nm.

## XI. SUMMARY PERSPECTIVE

Will OAM be widely deployed in communication systems? Not clear. However, our opinion is that the R&D community is producing excellent advances that, in all likelihood, will be valuable for some important aspects that use structured light.

This paper reviews the use of OAM to potentially enhance the capacity of MDM communication systems. The following points are noteworthy:

- (i) The use of OAM multiplexing under more complicated and harsher channel conditions than those described in this paper remains challenging. It would be important to investigate the system performance under these conditions and to develop potential techniques to combat the degradation effects. It would also be valuable to explore the limits of these conditions below which the degradation effects can be efficiently mitigated.
- (ii) The future of OAM deployment will rely heavily on the development of a technology ecosystem for OAM generation and multiplexing. Efficient OAM (de)multiplexing using compact and cost-efficient integrated devices would be one important issue.<sup>143</sup> Key desirable features of these integrated devices include<sup>68</sup> low insertion loss, high amplifier gain, uniform performance for different modes, high modal purity, low modal coupling and intermodal crosstalk, high efficiency for mode conversion, high dynamic range, small size, large wavelength range, and accommodation of high numbers of modes. Other functions that could be advantageous include (a) fast tunability and reconfigurability covering a range of OAM modes and (b) integration of an OAM communication system-on-a-chip that incorporates a full transceiver.
- (iii) OAM multiplexing could be utilized in different frequency domains. Future OAM systems might use hybrid technologies, and thus, systems that can be compatible with different OAM multiplexing technologies over different frequency domains may be valuable, including but not limited to the RF, mm-wave, THz, and optical domains.<sup>144–146</sup> Components, including broadband signal emitters/detectors

and frequency converters in different frequency domains, may need to be considered to enable heterogeneous OAM-multiplexed communications. Another consideration could be the frequency channel selections, the key challenges of which include link loss and channel distortion caused by OAM beam divergence and beam interaction with matter (e.g., atmospheric turbulence) in heterogeneous OAM-multiplexed links. In such cases, potential solutions, such as AO and MIMO, could be helpful.

## ACKNOWLEDGMENTS

We acknowledge the generous support from the Vannevar Bush Faculty Fellowship sponsored by the Basic Research Office of the Assistant Secretary of Defense (ASD) for Research and Engineering (R&E) and funded by the Office of Naval Research (ONR; Grant No. N00014-16-1-2813), the Defense Security Cooperation Agency (Grant No. DSCA 4441006051), the Air Force Research Laboratory (Grant No. FA8650-20-C-1105), the National Science Foundation (NSF; Grant No. ECCS-1509965), the Office of Naval Research through a MURI (Grant No. N00014-20-1-2558), the Airbus Institute for Engineering Research, the Nippon Telegraph and Telephone Corporation, and the Qualcomm Innovation Fellowship (QIF).

## DATA AVAILABILITY

The data that support the findings of this study are available from the corresponding author upon reasonable request.

## REFERENCES

- <sup>1</sup>L. Allen, M. W. Beijersbergen, R. J. C. Spreeuw, and J. P. Woerdman, *Phys. Rev. A* **45**, 8185 (1992).
- <sup>2</sup>R. L. Phillips and L. C. Andrews, *Appl. Opt.* **22**, 643 (1983).
- <sup>3</sup>A. M. Yao and M. J. Padgett, *Adv. Opt. Photonics* **3**, 161 (2011).
- <sup>4</sup>A. E. Willner, H. Huang, Y. Yan, Y. Ren, N. Ahmed, G. Xie, C. Bao, L. Li, Y. Cao, Z. Zhao, J. Wang, M. P. J. Lavery, M. Tur, S. Ramachandran, A. F. Molisch, N. Ashrafi, and S. Ashrafi, *Adv. Opt. Photonics* **7**, 66 (2015).
- <sup>5</sup>D. J. Richardson, J. M. Fini, and L. E. Nelson, *Nat. Photonics* **7**, 354 (2013).
- <sup>6</sup>P. J. Winzer, *Nat. Photonics* **8**, 345 (2014).
- <sup>7</sup>J. Wang, J.-Y. Yang, I. M. Fazal, N. Ahmed, Y. Yan, H. Huang, Y. Ren, Y. Yue, S. Dolinar, M. Tur, and A. E. Willner, *Nat. Photonics* **6**, 488 (2012).
- <sup>8</sup>Y. Yan, G. Xie, M. P. J. Lavery, H. Huang, N. Ahmed, C. Bao, Y. Ren, Y. Cao, L. Li, Z. Zhao, A. F. Molisch, M. Tur, M. J. Padgett, and A. E. Willner, *Nat. Commun.* **5**, 4876 (2014).
- <sup>9</sup>H. Huang, G. Xie, Y. Yan, N. Ahmed, Y. Ren, Y. Yue, D. Rogawski, M. J. Willner, B. I. Erkmen, K. M. Birnbaum, S. J. Dolinar, M. P. J. Lavery, M. J. Padgett, M. Tur, and A. E. Willner, *Opt. Lett.* **39**, 197 (2014).
- <sup>10</sup>J. Wang, S. Li, M. Luo, J. Liu, L. Zhu, C. Li, D. Xie, Q. Yang, S. Yu, J. Sun, X. Zhang, W. Shieh, and A. E. Willner, in *2014 The European Conference on Optical Communication (ECOC)* (ECOC, 2014), pp. 1–3.
- <sup>11</sup>A. E. Willner and C. Liu, *Nanophotonics* **10**, 225 (2020).
- <sup>12</sup>A. E. Willner, *IEEE Spectrum* **53**, 34 (2016).
- <sup>13</sup>Y. Ren, Z. Wang, P. Liao, L. Li, G. Xie, H. Huang, Z. Zhao, Y. Yan, N. Ahmed, A. Willner, M. P. J. Lavery, N. Ashrafi, S. Ashrafi, R. Bock, M. Tur, I. B. Djordjevic, M. A. Neifeld, and A. E. Willner, *Opt. Lett.* **41**, 622 (2016).
- <sup>14</sup>Y. Zhao, J. Liu, J. Du, S. Li, Y. Luo, A. Wang, L. Zhu, and J. Wang, in *2016 Optical Fiber Communications Conference and Exhibition (OFC)*, OSA Technical Digest (Optical Society of America, 2016), paper Th1H.3.
- <sup>15</sup>M. Krenn, J. Handsteiner, M. Fink, R. Fickler, R. Ursin, M. Malik, and A. Zeilinger, *Proc. Natl. Acad. Sci. U. S. A.* **113**, 13648 (2016).



- <sup>16</sup>N. Bozinovic, Y. Yue, Y. Ren, M. Tur, P. Kristensen, H. Huang, A. E. Willner, and S. Ramachandran, *Science* **340**, 1545 (2013).
- <sup>17</sup>K. Pang, H. Song, Z. Zhao, R. Zhang, H. Song, G. Xie, L. Li, C. Liu, J. Du, A. F. Molisch, M. Tur, and A. E. Willner, *Opt. Lett.* **43**, 3889 (2018).
- <sup>18</sup>G. Xie, Y. Ren, Y. Yan, H. Huang, N. Ahmed, L. Li, Z. Zhao, C. Bao, M. Tur, S. Ashrafi, and A. E. Willner, *Opt. Lett.* **41**, 3447 (2016).
- <sup>19</sup>R. Ryf, S. Randel, A. H. Gnauck, C. Bolle, A. Sierra, S. Mumtaz, M. Esmaelpour, E. C. Burrows, R.-J. Essiambre, P. J. Winzer, D. W. Peckham, A. H. McCurdy, and R. Lingle, *J. Lightwave Technol.* **30**, 521 (2012).
- <sup>20</sup>B. Ndagano, R. Brünig, M. McLaren, M. Duparré, and A. Forbes, *Opt. Express* **23**, 17330 (2015).
- <sup>21</sup>R. W. Boyd and M. J. Padgett, private communication (2020).
- <sup>22</sup>M. J. Padgett, R. W. Boyd, and A. E. Willner, private communication (2020).
- <sup>23</sup>S. Restuccia, D. Giovannini, G. Gibson, and M. Padgett, *Opt. Express* **24**, 27127 (2016).
- <sup>24</sup>L. Li, G. Xie, Y. Yan, Y. Ren, P. Liao, Z. Zhao, N. Ahmed, Z. Wang, C. Bao, A. J. Willner, S. Ashrafi, M. Tur, and A. E. Willner, *J. Opt. Soc. Am. B* **34**, 1 (2017).
- <sup>25</sup>G. Gibson, J. Courtial, M. J. Padgett, M. Vasnetsov, V. Pas'ko, S. M. Barnett, and S. Franke-Arnold, *Opt. Express* **12**, 5448 (2004).
- <sup>26</sup>L. C. Andrews and R. L. Phillips, *Laser Beam Propagation Through Random Media* (SPIE, 2005).
- <sup>27</sup>G. A. Tyler and R. W. Boyd, *Opt. Lett.* **34**, 142 (2009).
- <sup>28</sup>Y. Ren, H. Huang, G. Xie, N. Ahmed, Y. Yan, B. I. Erkmen, N. Chandrasekaran, M. P. J. Lavery, N. K. Steinhoff, M. Tur, S. Dolinar, M. Neifeld, M. J. Padgett, R. W. Boyd, J. H. Shapiro, and A. E. Willner, *Opt. Lett.* **38**, 4062 (2013).
- <sup>29</sup>S. Fu and C. Gao, *Photonics Res.* **4**, B1 (2016).
- <sup>30</sup>G. Xie, L. Li, Y. Ren, H. Huang, Y. Yan, N. Ahmed, Z. Zhao, M. P. J. Lavery, N. Ashrafi, S. Ashrafi, R. Bock, M. Tur, A. F. Molisch, and A. E. Willner, *Optica* **2**, 357 (2015).
- <sup>31</sup>X. Zhong, Y. Zhao, G. Ren, S. He, and Z. Wu, *IEEE Access* **6**, 8742 (2018).
- <sup>32</sup>Z. Mei and D. Zhao, *J. Opt. A: Pure Appl. Opt.* **6**, 1005 (2004).
- <sup>33</sup>G. Labroille, B. Denolle, P. Jian, P. Genevieux, N. Treps, and J.-F. Morizur, *Opt. Express* **22**, 15599–15607 (2014).
- <sup>34</sup>N. K. Fontaine, R. Ryf, H. Chen, D. T. Neilson, K. Kim, and J. Carpenter, *Nat. Commun.* **10**(1), 1865 (2019).
- <sup>35</sup>Y. Wen, I. Chremmos, Y. Chen, J. Zhu, Y. Zhang, and S. Yu, *Phys. Rev. Lett.* **120**(19), 193904 (2018).
- <sup>36</sup>G. C. Berkhout, M. P. J. Lavery, J. Courtial, M. W. Beijersbergen, and M. J. Padgett, *Phys. Rev. Lett.* **105**(15), 153601 (2010).
- <sup>37</sup>Z. S. Eznavah, J. C. A. Zacarias, J. E. A. Lopez, K. Shi, G. Milione, Y. Jung, B. C. Thomsen, D. J. Richardson, N. Fontaine, S. G. Leon-Saval, and R. A. Correa, *Opt. Express* **26**(23), 30042–30051 (2018).
- <sup>38</sup>J. A. Anguita, M. A. Neifeld, and B. V. Vasic, *Appl. Opt.* **47**, 2414 (2008).
- <sup>39</sup>N. Chandrasekaran and J. H. Shapiro, *J. Lightwave Technol.* **32**, 1075 (2014).
- <sup>40</sup>C. Paterson, *Phys. Rev. Lett.* **94**, 153901 (2005).
- <sup>41</sup>M. Malik, M. O'Sullivan, B. Rodenburg, M. Mirhosseini, J. Leach, M. P. J. Lavery, M. J. Padgett, and R. W. Boyd, *Opt. Express* **20**, 13195 (2012).
- <sup>42</sup>Y. Ren, G. Xie, H. Huang, C. Bao, Y. Yan, N. Ahmed, M. P. J. Lavery, B. I. Erkmen, S. Dolinar, M. Tur, M. A. Neifeld, M. J. Padgett, R. W. Boyd, J. H. Shapiro, and A. E. Willner, *Opt. Lett.* **39**, 2845 (2014).
- <sup>43</sup>K. Pang, S. Haoqian, X. Su, K. Zou, Z. Zhao, H. Song, A. Almainan, R. Zhang, C. Liu, N. Hu, S. Zach, N. Cohen, B. Lynn, A. F. Molisch, R. W. Boyd, M. Tur, and A. E. Willner, in *2020 Optical Fiber Communications Conference and Exhibition (OFC)*, OSA Technical Digest (Optical Society of America, 2020), pp. 1–3.
- <sup>44</sup>G. A. Tyler, *Opt. Eng.* **52**, 021011 (2012).
- <sup>45</sup>Y. Ren, G. Xie, H. Huang, N. Ahmed, Y. Yan, L. Li, C. Bao, M. P. J. Lavery, M. Tur, M. A. Neifeld, R. W. Boyd, J. H. Shapiro, and A. E. Willner, *Optica* **1**, 376 (2014).
- <sup>46</sup>S. Chen, S. Li, Y. Zhao, J. Liu, L. Zhu, A. Wang, J. Du, L. Shen, and J. Wang, *Opt. Lett.* **41**(20), 4680–4683 (2016).
- <sup>47</sup>P. J. Winzer and G. J. Foschini, *Opt. Express* **19**, 16680 (2011).
- <sup>48</sup>B. Clerckx and C. Oestges, *MIMO Wireless Networks: Channels, Techniques and Standards for Multi-Antenna, Multi-User and Multi-Cell Systems* (Academic Press, 2013).
- <sup>49</sup>H. Huang, Y. Cao, G. Xie, Y. Ren, Y. Yan, C. Bao, N. Ahmed, M. A. Neifeld, S. J. Dolinar, and A. E. Willner, *Opt. Lett.* **39**, 4360 (2014).
- <sup>50</sup>R. Fickler, M. Ginoya, and R. W. Boyd, *Phys. Rev. B* **95**, 161108 (2017).
- <sup>51</sup>I. M. Vellekoop and A. P. Mosk, *Phys. Rev. Lett.* **101**, 120601 (2008).
- <sup>52</sup>R. Zhang, H. Song, Z. Zhao, H. Song, J. Du, C. Liu, K. Pang, L. Li, H. Zhou, A. N. Willner, A. Almainan, Y. Zhou, R. W. Boyd, B. Lynn, R. Bock, M. Tur, and A. E. Willner, *Opt. Lett.* **45**, 702–705 (2020).
- <sup>53</sup>J.-F. Morizur, L. Nicholls, P. Jian, S. Armstrong, N. Treps, B. Hage, M. Hsu, W. Bowen, J. Janousek, and H.-A. Bachor, *J. Opt. Soc. Am. A* **27**, 2524–2531 (2010).
- <sup>54</sup>H. Song, X. Su, H. Song, R. Zhang, Z. Zhao, C. Liu, K. Pang, N. Hu, A. Almainan, S. Zach, N. Cohen, A. Molisch, R. Boyd, M. Tur, and A. E. Willner, in *2020 Optical Fiber Communications Conference (OFC)*, OSA Technical Digest (Optical Society of America, 2020), p. W1G.3.
- <sup>55</sup>H. Song, H. Song, R. Zhang, K. Manukyan, L. Li, Z. Zhao, K. Pang, C. Liu, A. Almainan, R. Bock, B. Lynn, M. Tur, and A. E. Willner, *J. Lightwave Technol.* **38**, 82 (2020).
- <sup>56</sup>D. A. B. Miller, *Science* **347**, 1423 (2015).
- <sup>57</sup>V. Liu, D. A. B. Miller, and S. Fan, *Opt. Express* **20**, 28388 (2012).
- <sup>58</sup>C. Yang, C. Xu, W. Ni, Y. Gan, J. Hou, and S. Chen, *Opt. Express* **25**, 25612 (2017).
- <sup>59</sup>L. Li, R. Zhang, Z. Zhao, G. Xie, P. Liao, K. Pang, H. Song, C. Liu, Y. Ren, G. Labroille, P. Jian, D. Starodubov, B. Lynn, R. Bock, M. Tur, and A. E. Willner, *Sci. Rep.* **7**, 17427 (2017).
- <sup>60</sup>J. Cunningham, D. Foulke, T. Goode, D. Baber, B. Gaughan, M. Fletcher, D. W. Young, J. C. Juarez, J. E. Sluz, and J. L. Riggins, in *MILCOM 2009—2009 IEEE Military Communications Conference* (IEEE, 2009), pp. 1–7.
- <sup>61</sup>S. S. Muhammad, T. Plank, E. Leitgeb, A. Friedl, K. Zettl, T. Javornik, and N. Schmitt, in *2008 6th International Symposium on Communication Systems, Networks and Digital Signal Processing* (IEEE, 2008), pp. 82–86.
- <sup>62</sup>R. Fields, C. Lunde, R. Wong, J. Wicker, D. Kozlowski, J. Jordan, B. Hansen, G. Muehlhnickel, W. Scheel, U. Sterr, R. Kahle, and R. Meyer, *Proc. SPIE* **7330**, 73300Q (2009).
- <sup>63</sup>F. Heine, G. Muehlhnickel, H. Zech, S. Philipp-May, and R. Meyer, in *2014 7th Advanced Satellite Multimedia Systems Conference and the 13th Signal Processing for Space Communications Workshop (ASMS/SPSC)* (IEEE, 2014), pp. 284–286.
- <sup>64</sup>F. Moll, J. Horwath, A. Shrestha, M. Brechtelsbauer, C. Fuchs, L. A. Martin Navajas, A. M. Lozano Souto, and D. Díaz González, *IEEE J. Sel. Areas Commun.* **33**, 1985 (2015).
- <sup>65</sup>K. E. Zarganis and A. Hatziefremidis, *Am. J. Opt. Photonics* **3**, 5 (2015).
- <sup>66</sup>A. Kaadan, H. Refai, and P. Lopresti, *IEEE Trans. Aerosp. Electron. Syst.* **52**, 2157 (2016).
- <sup>67</sup>A. Kaadan, H. H. Refai, and P. G. LoPresti, *J. Lightwave Technol.* **32**, 4785 (2014).
- <sup>68</sup>A. E. Willner, in *Conference on Lasers and Electro-Optics*, Paper STu3B.1 (Optical Society of America, 2018).
- <sup>69</sup>K. Kazaura, K. Omae, T. Suzuki, M. Matsumoto, E. Mutaungwa, T. O. Korhonen, T. Murakami, K. Takahashi, H. Matsumoto, K. Wakamori, and Y. Arimoto, *Opt. Express* **14**, 4958 (2006).
- <sup>70</sup>L. Li, R. Zhang, G. Xie, Y. Ren, Z. Zhao, Z. Wang, C. Liu, H. Song, K. Pang, R. Bock, M. Tur, and A. E. Willner, *Opt. Lett.* **43**, 2392 (2018).
- <sup>71</sup>L. Li, R. Zhang, P. Liao, Y. Cao, H. Song, Y. Zhao, J. Du, Z. Zhao, C. Liu, K. Pang, H. Song, A. Almainan, D. Starodubov, B. Lynn, R. Bock, M. Tur, A. F. Molisch, and A. E. Willner, *Opt. Lett.* **44**, 5181 (2019).
- <sup>72</sup>E. Ciaramella, Y. Arimoto, G. Contestabile, M. Presi, A. D'Errico, V. Guarino, and M. Matsumoto, *IEEE J. Sel. Areas Commun.* **27**, 1639 (2009).
- <sup>73</sup>G. Xie, L. Li, Y. Ren, Y. Yan, N. Ahmed, Z. Zhao, C. Bao, Z. Wang, C. Liu, H. Song, R. Zhang, K. Pang, S. Ashrafi, M. Tur, and A. E. Willner, *Opt. Lett.* **42**, 395 (2017).
- <sup>74</sup>N. Friedman, *The Naval Institute Guide to World Naval Weapon Systems* (Naval Institute Press, 2006).

- <sup>75</sup>M. Stojanovic, *IEEE J. Oceanic Eng.* **21**, 125 (1996).
- <sup>76</sup>J. Wang, C. Lu, S. Li, and Z. Xu, *Opt. Express* **27**, 12171 (2019).
- <sup>77</sup>J. Baghdady, K. Miller, K. Morgan, M. Byrd, S. Osler, R. Ragusa, W. Li, B. M. Cochenour, and E. G. Johnson, *Opt. Express* **24**, 9794 (2016).
- <sup>78</sup>Y. Ren, L. Li, Z. Wang, S. M. Kamali, E. Arbabi, A. Arbabi, Z. Zhao, G. Xie, Y. Cao, N. Ahmed, Y. Yan, C. Liu, A. J. Willner, S. Ashrafi, M. Tur, A. Faraon, and A. E. Willner, *Sci. Rep.* **6**, 33306 (2016).
- <sup>79</sup>A. K. Majumdar, J. Siegenthaler, and P. Land, *Proc. SPIE* **8517**, 85170T (2012).
- <sup>80</sup>R. F. Lutomirski, *Proc. SPIE* **160**, 110–122 (1978).
- <sup>81</sup>M. Cheng, L. Guo, and Y. Zhang, *Opt. Express* **23**, 32606–32621 (2015).
- <sup>82</sup>Y. Zhao, A. Wang, L. Zhu, W. Lv, J. Xu, S. Li, and J. Wang, *Opt. Lett.* **42**(22), 4699–4702 (2017).
- <sup>83</sup>D. McGloin and K. Dholakia, *Contemp. Phys.* **46**, 15 (2005).
- <sup>84</sup>N. K. Efremidis, Z. Chen, M. Segev, and D. N. Christodoulides, *Optica* **6**, 686–701 (2019).
- <sup>85</sup>G. Zhu, Y. Wen, X. Wu, Y. Chen, J. Liu, and S. Yu, *Opt. Lett.* **43**, 1203–1206 (2018).
- <sup>86</sup>L. Zhu, A. Wang, and J. Wang, *Sci. Rep.* **9**, 14969 (2019).
- <sup>87</sup>L. Zhu, Z. Yang, S. Fu, Z. Cao, Y. Wang, Y. Qin, and A. M. J. Koonen, *J. Lightwave Technol.* **38**, 6474–6480 (2020).
- <sup>88</sup>N. Ahmed, Z. Zhao, L. Li, H. Huang, M. P. J. Lavery, P. Liao, Y. Yan, Z. Wang, G. Xie, Y. Ren, A. Alaiman, A. J. Willner, S. Ashrafi, A. F. Molisch, M. Tur, and A. E. Willner, *Sci. Rep.* **6**, 22082 (2016).
- <sup>89</sup>M. Erhard, R. Fickler, M. Krenn, and A. Zeilinger, *Light: Sci. Appl.* **7**, 17146 (2018).
- <sup>90</sup>M. Mirhosseini, O. S. Magaña-Loaiza, M. N. O'Sullivan, B. Rodenburg, M. Malik, M. P. J. Lavery, M. J. Padgett, D. J. Gauthier, and R. W. Boyd, *New J. Phys.* **17**, 033033 (2015).
- <sup>91</sup>M. Mafu, A. Dudley, S. Goyal, D. Giovannini, M. McLaren, M. J. Padgett, T. Konrad, F. Petruccione, N. Lütkenhaus, and A. Forbes, *Phys. Rev. A* **88**, 032305 (2013).
- <sup>92</sup>C. Liu, K. Pang, Z. Zhao, P. Liao, R. Zhang, H. Song, Y. Cao, J. Du, L. Li, H. Song, Y. Ren, G. Xie, Y. Zhao, J. Zhao, S. M. H. Rafsanjani, A. N. Willner, J. H. Shapiro, R. W. Boyd, M. Tur, and A. E. Willner, *Research* **2019**, 8326701.
- <sup>93</sup>J. Liu, I. Nape, Q. Wang, A. Vallés, J. Wang, and A. Forbes, *Sci. Adv.* **6**(4), eaay0837 (2020).
- <sup>94</sup>C. H. Bennett and G. Brassard, *Theor. Comput. Sci.* **560**, 7 (2014).
- <sup>95</sup>H. Hübel, M. R. Vanner, T. Lederer, B. Blauensteiner, T. Lörünser, A. Poppe, and A. Zeilinger, *Opt. Express* **15**, 7853 (2007).
- <sup>96</sup>C.-Z. Peng, J. Zhang, D. Yang, W.-B. Gao, H.-X. Ma, H. Yin, H.-P. Zeng, T. Yang, X.-B. Wang, and J.-W. Pan, *Phys. Rev. Lett.* **98**, 010505 (2007).
- <sup>97</sup>S.-K. Liao, W.-Q. Cai, W.-Y. Liu, L. Zhang, Y. Li, J.-G. Ren, J. Yin, Q. Shen, Y. Cao, Z.-P. Li, F.-Z. Li, X.-W. Chen, L.-H. Sun, J.-J. Jia, J.-C. Wu, X.-J. Jiang, J.-F. Wang, Y.-M. Huang, Q. Wang, Y.-L. Zhou, L. Deng, T. Xi, L. Ma, T. Hu, Q. Zhang, Y.-A. Chen, N.-L. Liu, X.-B. Wang, Z.-C. Zhu, C.-Y. Lu, R. Shu, C.-Z. Peng, J.-Y. Wang, and J.-W. Pan, *Nature* **549**, 43 (2017).
- <sup>98</sup>G. Vallone, V. D'Ambrosio, A. Sponselli, S. Slussarenko, L. Marrucci, F. Sciarrino, and P. Villoresi, *Phys. Rev. Lett.* **113**, 060503 (2014).
- <sup>99</sup>F. Bouchard, A. Sit, F. Hufnagel, A. Abbas, Y. Zhang, K. Heshami, R. Fickler, C. Marquardt, G. Leuchs, R. W. Boyd, and E. Karimi, *Opt. Express* **26**, 22563 (2018).
- <sup>100</sup>D. Cozzolino, E. Polino, M. Valeri, G. Carvacho, D. Bacco, N. Spagnolo, L. K. Oxenløwe, and F. Sciarrino, *Adv. Photonics* **1**(4), 046005 (2019).
- <sup>101</sup>H. Cao, S. C. Gao, C. Zhang, J. Wang, D. Y. He, B. H. Liu, Z. W. Zhou, Y. J. Chen, Z. H. Li, S. Y. Yu, J. Romero, Y. F. Huang, C.-F. Li, and G.-C. Guo, *Optica* **7**(3), 232–237 (2020).
- <sup>102</sup>A. Sit, F. Bouchard, R. Fickler, J. Gagnon-Bischoff, H. Larocque, K. Heshami, D. Elser, C. Peuntinger, K. Günthner, B. Heim, C. Marquardt, G. Leuchs, R. W. Boyd, and E. Karimi, *Optica* **4**, 1006 (2017).
- <sup>103</sup>M. Hillery, V. Bužek, and A. Berthiaume, *Phys. Rev. A* **59**, 1829 (1999).
- <sup>104</sup>W. Tittel, H. Zbinden, and N. Gisin, *Phys. Rev. A* **63**, 042301 (2001).
- <sup>105</sup>Y.-A. Chen, A.-N. Zhang, Z. Zhao, X.-Q. Zhou, C.-Y. Lu, C.-Z. Peng, T. Yang, and J.-W. Pan, *Phys. Rev. Lett.* **95**, 200502 (2005).
- <sup>106</sup>J. Pinnell, I. Nape, M. de Oliveira, N. TabeBordbar, and A. Forbes, *Laser Photonics Rev.* **14**, 2000012 (2020).
- <sup>107</sup>C. Shi, M. Dubois, Y. Wang, and X. Zhang, *Proc. Natl. Acad. Sci. U. S. A.* **114**, 7250 (2017).
- <sup>108</sup>W. Cheng, H. Zhang, L. Liang, H. Jing, and Z. Li, *IEEE Access* **6**, 2732 (2018).
- <sup>109</sup>D. Lee, H. Sasaki, H. Fukumoto, Y. Yagi, and T. Shimizu, *Appl. Sci.* **9**, 1729 (2019).
- <sup>110</sup>H. Sasaki, D. Lee, H. Fukumoto, Y. Yagi, T. Kaho, H. Shiba, and T. Shimizu, in *2018 IEEE Global Communications Conference (GLOBECOM)* (IEEE, 2018), pp. 1–6.
- <sup>111</sup>H. Sasaki, Y. Yagi, T. Yamada, and D. Lee, in *2019 IEEE Globecom Workshops (GC Wkshps)* (IEEE, 2019), pp. 1–4.
- <sup>112</sup>Z. Zhao, Y. Yan, L. Li, G. Xie, Y. Ren, N. Ahmed, Z. Wang, C. Liu, A. J. Willner, P. Song, H. Hashemi, H. Yao, D. Macfarlane, R. Henderson, N. Ashrafi, S. Ashrafi, S. Talwar, S. Sajuyigbe, M. Tur, A. F. Molisch, and A. E. Willner, in *2016 IEEE International Conference on Communications (ICC)* (IEEE, 2016), pp. 1–6.
- <sup>113</sup>G. Xie, Z. Zhao, Y. Yan, L. Li, Y. Ren, N. Ahmed, Y. Cao, A. J. Willner, C. Bao, Z. Wang, C. Liu, M. Ziyadi, S. Talwar, S. Sajuyigbe, S. Ashrafi, M. Tur, A. F. Molisch, and A. E. Willner, *Sci. Rep.* **6**, 37078 (2016).
- <sup>114</sup>X. Wei, L. Zhu, Z. Zhang, K. Wang, J. Liu, and J. Wang, in *CLEO: 2014, Paper STu2F.2* (Optical Society of America, 2014).
- <sup>115</sup>C. Liu, X. Wei, L. Niu, K. Wang, Z. Yang, and J. Liu, *Opt. Express* **24**, 12534 (2016).
- <sup>116</sup>Q. Wu and R. Zhang, *IEEE Trans. Wireless Commun.* **18**, 5394–5409 (2019).
- <sup>117</sup>X. G. Zhang, W. X. Jiang, H. L. Jiang, Q. Wang, H. W. Tian, L. Bai, Z. J. Luo, S. Sun, Y. Luo, C.-W. Qiu, and T. J. Cui, *Nat. Electron.* **3**(3), 165–171 (2020).
- <sup>118</sup>C. M. Watts, D. Shrekenhamer, J. Montoya, G. Lipworth, J. Hunt, T. Sleasman, S. Krishna, D. R. Smith, and W. J. Padilla, *Nat. Photonics* **8**(8), 605–609 (2014).
- <sup>119</sup>X. Hui, S. Zheng, Y. Chen, Y. Hu, X. Jin, H. Chi, and X. Zhang, *Sci. Rep.* **5**, 10148 (2015).
- <sup>120</sup>Y. Yan, L. Li, Z. Zhao, G. Xie, Z. Wang, Y. Ren, N. Ahmed, S. Sajuyigbe, S. Talwar, M. Tur, N. Ashrafi, S. Ashrafi, A. F. Molisch, and A. E. Willner, in *2016 IEEE International Conference on Communications (ICC)* (IEEE, 2016), pp. 1–6.
- <sup>121</sup>W. Wei, K. Mahdjoubi, C. Brousseau, and O. Emile, *Electron. Lett.* **51**, 442 (2015).
- <sup>122</sup>Z. Zhao, G. Xie, L. Li, H. Song, C. Liu, K. Pang, R. Zhang, C. Bao, Z. Wang, S. Sajuyigbe, S. Talwar, H. Nikopour, and A. E. Willner, in *GLOBECOM 2017–2017 IEEE Global Communications Conference* (IEEE, 2017), pp. 1–6.
- <sup>123</sup>Z. Zhao, Y. Ren, G. Xie, Y. Yan, L. Li, H. Huang, C. Bao, N. Ahmed, M. P. Lavery, C. Zhang, N. Ashrafi, S. Ashrafi, S. Talwar, S. Sajuyigbe, M. Tur, A. F. Molisch, and A. E. Willner, in *2015 IEEE International Conference on Communications (ICC)* (IEEE, 2015), pp. 1392–1397.
- <sup>124</sup>Z. Zhao, R. Zhang, H. Song, K. Pang, A. Alaiman, H. Zhou, H. Song, C. Liu, N. Hu, X. Su, A. Minoofar, S. Zach, N. Cohen, M. Tur, A. Molisch, and A. E. Willner, in *ICC 2020–2020 IEEE International Conference on Communications (ICC)* (IEEE, 2020), pp. 1–7.
- <sup>125</sup>X. Su, R. Zhang, Z. Zhao, H. Song, A. Minoofar, N. Hu, H. Zhou, K. Zou, K. Pang, H. Song, B. Lynn, S. Zach, N. Cohen, M. Tur, A. Molisch, H. Sasaki, D. Lee, and A. E. Willner, in *2020 IEEE Globecom Workshops (GC Wkshps)* (IEEE, 2020), pp. 1–6.
- <sup>126</sup>R. W. Heath, Jr., N. Gonzalez-Prelcic, S. Rangan, W. Roh, and A. M. Sayeed, *IEEE J. Sel. Top. Signal Process.* **10**, 436 (2016).
- <sup>127</sup>O. E. Ayach, S. Rajagopal, S. Abu-Surra, Z. Pi, and R. W. Heath, *IEEE Trans. Wireless Commun.* **13**, 1499 (2014).
- <sup>128</sup>Y. Ren, L. Li, G. Xie, Y. Yan, Y. Cao, H. Huang, N. Ahmed, Z. Zhao, P. Liao, C. Zhang, G. Caire, A. F. Molisch, M. Tur, and A. E. Willner, *IEEE Trans. Wireless Commun.* **16**, 3151 (2017).
- <sup>129</sup>B. Palacin, K. Sharshavina, K. Nguyen, and N. Capet, in *The 8th European Conference on Antennas and Propagation (EuCAP 2014)* (European Association on Antennas and Propagation, 2014), pp. 2814–2818.

- <sup>130</sup>H. Sasaki, Y. Yagi, T. Yamada, T. Semoto, and D. Lee, in *2020 IEEE International Conference on Communications Workshops (ICC Workshops)* (IEEE, 2020), pp. 1–6.
- <sup>131</sup>R. Zhang, H. Song, H. Song, Z. Zhao, G. Milione, K. Pang, J. Du, L. Li, K. Zou, H. Zhou, C. Liu, K. Manukyan, N. Hu, A. Almainan, J. Stone, M.-J. Li, B. Lynn, R. W. Boyd, M. Tur, and A. E. Willner, *Opt. Lett.* **45**, 3577 (2020).
- <sup>132</sup>J. Carpenter, B. C. Thomsen, and T. D. Wilkinson, *J. Lightwave Technol.* **30**, 3946 (2012).
- <sup>133</sup>K.-i. Kitayama and N.-P. Diamantopoulos, *IEEE Commun. Mag.* **55**, 163 (2017).
- <sup>134</sup>S. Randel, R. Ryf, A. Sierra, P. J. Winzer, A. H. Gnauck, C. A. Bolle, R.-J. Essiambre, D. W. Peckham, A. McCurdy, and R. Lingle, *Opt. Express* **19**, 16697 (2011).
- <sup>135</sup>C. Brunet, P. Vaity, Y. Messaddeq, S. LaRochelle, and L. A. Rusch, *Opt. Express* **22**, 26117 (2014).
- <sup>136</sup>S. Bae, Y. Jung, B. G. Kim, and Y. C. Chung, *IEEE Photonics Technol. Lett.* **31**, 739 (2019).
- <sup>137</sup>J. Zhang, J. Liu, L. Shen, L. Zhang, J. Luo, J. Liu, and S. Yu, *Photonics Res.* **8**(7), 1236–1242 (2020).
- <sup>138</sup>J. Liu, S.-M. Li, L. Zhu, A.-D. Wang, S. Chen, C. Klitis, C. Du, Q. Mo, M. Sorel, S.-Y. Yu, X.-L. Cai, and J. Wang, *Light: Sci. Appl.* **7**(3), 17148 (2018).
- <sup>139</sup>N. Riesen, J. D. Love, and J. W. Arkwright, *IEEE Photonics Technol. Lett.* **24**, 344 (2012).
- <sup>140</sup>Y. Jung, Q. Kang, R. Sidharthan, D. Ho, S. Yoo, P. Gregg, S. Ramachandran, S.-U. Alam, and D. J. Richardson, *J. Lightwave Technol.* **35**, 430 (2017).
- <sup>141</sup>J. Liu, S. Chen, H. Wang, S. Zheng, L. Zhu, A. Wang, L. Wang, C. Du, and J. Wang, *Research* **2020**, 7623751.
- <sup>142</sup>L. Zhu, J. Li, G. Zhu, L. Wang, C. Cai, A. Wang, S. Li, M. Tang, Z. He, S. Yu, S. Yu, C. Du, W. Luo, J. Liu, J. Du, and J. Wang, in *Optical Fiber Communication Conference (2018)*, Paper W4C.4 (Optical Society of America, 2018).
- <sup>143</sup>N. Zhou, S. Zheng, X. Cao, Y. Zhao, S. Gao, Y. Zhu, M. He, X. Cai, and J. Wang, *Sci. Adv.* **5**(5), eaau9593 (2019).
- <sup>144</sup>F. Nadeem, V. Kvicera, M. S. Awan, E. Leitgeb, S. S. Muhammad, and G. Kandus, *IEEE J. Sel. Areas Commun.* **27**, 1687–1697 (2009).
- <sup>145</sup>A. Trichili, M. A. Cox, B. S. Ooi, and M.-S. Alouini, *J. Opt. Soc. Am. B* **37**, A184–A201 (2020).
- <sup>146</sup>F. Ahdi and S. Subramaniam, in *2011 IEEE Global Telecommunications Conference (GLOBECOM)* (IEEE, 2011), pp. 1–6.